UNIVERSITY OF CONCEPCION

FACULTY OF ENGINEERING

ELECTRICAL ENGINEERING DEPARTMENT

BASELINE CORRECTION ALGORITHM FOR QUANTIFICATION OF IN VIVO ^{1}H-MRS

BY

Diego Alejandro Pasmiño Ceballos

A thesis submitted to the Faculty of Engineering of the University of Concepcion for the degree of Master of Science in Electrical Engineering.

Advisor 1

Sc.D. Esteban Pino Quiroga.

Advisor 2

Ph.D. Pamela Guevara Alvez.

External advisor 1

Ph.D. Johannes Slotboom

External advisor 2

Ph.D. Waldo Valenzuela Pinilla.

October 2023

Concepción, Chile

Acknowledgements

Firstly, I would like to thank my thesis advisor, Sc.D. Esteban Pino Quiroga, who supported me unconditionally throughout the course of this work. His advice was of great help in overcoming the challenges that arose, allowing me to progress in a rather difficult yet highly interesting area of science.

I would also like to express my gratitude to Professor Ph.D. Johannes Slotboom from the University Hospital of Bern, Switzerland, without whose extraordinary assistance this work would have never been completed. Alongside him, I extend my thanks to another member of the Support Center for Advance Neuroimaging (SCAN) team, Federico Turco, who assisted me in preprocessing the data used in this thesis.

Furthermore, I am immensely grateful for the guidance of my mentor, Brigitte Schweisthal, who played a significant role in the study of the art in this work. I also want to thank professors Ph.D. Pamela Guevara and Ph.D. Waldo Valenzuela, who actively responded to the questions I had, were always happy to cooperate.

Finally, I would like to thank my family and friends, who accompanied me at all times during the many years it took to complete this thesis. In moments of joy and especially in those times of great sadness that often made me doubt finishing this work, they always supported me and encouraged me to continue.

Thank you very much, everyone.

Abstract

Proton Magnetic Resonance Spectroscopy (^{1}H-MRS) is used by clinicians to study diseases by obtaining detailed information on the intra- and extra-cellular biochemical components. This technique provides unique ways for disease diagnosis. However, one of its remaining problems is the absence of a reliable algorithm for baseline correction, sometimes considered one of the largest sources of uncertainty for *in vivo* Magnetic Resonance Spectroscopy (MRS) quantification. Baselines commonly appear in signals with short echo time (TE) and poorly shimmed volume of interest (VOI), as with ^{1}H-MRS signals. In the last two decades, many baseline estimation methods have been proposed. These algorithms are based on different mathematical approaches, such as cubic spline interpolation, smoothing filters, wavelets, and penalised least squares, among others. Although some approaches are good for estimating the absorption component of the baseline, most of them do not perform well for the complex MRS signal. This leads to problems at the quantification step, resulting in non-reliable data and possibly study failure. This thesis proposes a novel method for baseline correction that combines time-domain (TD) and frequency-domain (FD) processing of the MRS data. To identify where and how to include this processing, a testing step was proposed, where state-of-the-art (SOTA) algorithms were compared by using real signals with simulated baselines, i.e. with ground truth data. The proposed method obtained, on average, better RMSE than two of the four SOTA algorithms. The proposed novel method was later compared using fourteen real datasets from anonymised patients. The comparison metric proposed in this project is the Fit Quality Number (FQN), where only the baseline correction performance was compared, using the same preprocessing and quantification method for every tested algorithm. The results of the novel proposal show an efficient performance when combining methods in TD and FD for baseline correction, achieving better results than the four SOTA algorithms that were compared in this evaluation, with the advantage of correcting the complex signal, instead of only estimating the baseline for the absorption spectrum. Further work should be focused on improving the performance of the algorithm.

Keywords — *in vivo* ^{1}H-MRS, MRS, MRI, CSI, MRSI, baseline correction

Resumen

La Espectroscopia de Resonancia Magnética Protonica (^{1}H-MRS) es utilizada por los clínicos para estudiar enfermedades al obtener información detallada sobre los componentes bioquímicos intra y extra celulares. Esta técnica proporciona formas únicas de diagnóstico de enfermedades. Sin embargo, uno de sus problemas pendientes es la falta de un algoritmo confiable para la corrección de la línea de base, a menudo considerada una de las fuentes más grandes de incertidumbre en la cuantificación de Espectroscopia de Resonancia Magnética *in vivo* (MRS). Las líneas de base comúnmente aparecen en señales con un tiempo de eco (TE) corto y un volumen de interés (VOI) mal ajustado, como en las señales de ^{1}H-MRS. En las últimas dos décadas, se han propuesto muchos métodos de estimación de la línea de base. Estos algoritmos se basan en diferentes enfoques matemáticos, como la interpolación cúbica spline, filtros de suavizado, wavelets y mínimos cuadrados penalizados, entre otros. Aunque algunos enfoques son buenos para estimar el componente de absorción de la línea de base, la mayoría de ellos no funcionan bien para la señal compleja de MRS. Esto conlleva problemas en la etapa de cuantificación, lo que resulta en datos no confiables y posiblemente en el fracaso del estudio. Esta tesis propone un método novedoso para la corrección de la línea de base que combina el procesamiento en el dominio del tiempo (TD) y en el dominio de la frecuencia (FD) de los datos de MRS. Para identificar dónde y cómo incluir este procesamiento, se propuso una etapa de prueba, donde se compararon algoritmos de última generación (SOTA) utilizando señales reales con líneas de base simuladas, es decir, con datos de referencia. El método propuesto obtuvo, en promedio, un RMSE mejor que dos de los cuatro algoritmos SOTA. El método novedoso propuesto se comparó posteriormente utilizando catorce conjuntos de datos reales de pacientes anonimizados. La métrica de comparación propuesta en este proyecto es el Número de Calidad de Ajuste (FQN), donde solo se comparó el rendimiento de la corrección de la línea de base, utilizando el mismo procesamiento previo y método de cuantificación para cada algoritmo probado. Los resultados de la propuesta novedosa muestran un rendimiento eficiente al combinar métodos en TD y FD para la corrección de la línea de base, logrando mejores resultados que los cuatro algoritmos SOTA que se compararon en esta evaluación, con la ventaja de corregir la señal compleja en lugar de solo estimar la línea de base para el espectro de absorción. El trabajo futuro debería centrarse en mejorar el rendimiento del algoritmo.

Table of Contents

Abbreviations **VI**

List of Tables **VIII**

List of Figures **IX**

1. Chapter 1. Introduction **1**

1.1. Main introduction 1

1.2. Hypothesis 3

1.3. Objectives 3

1.4. Methodology 3

1.5. Scope and limitations 5

2. Chapter 2. State of the Art **6**

2.1. Magnetic resonance spectroscopy 6

2.2. Signal acquisition and preprocessing 7

2.3. Artefacts in in vivo 1H-MRS spectra and characterisation of baseline. 10

2.4. Baseline correction for in vivo 1H-MRS and general NMR spectra 11

2.5. Validation and comparison methods 16

2.6. Discussion 19

3. Chapter 3. Testing SOTA algorithms and design of the proposed algorithm **21**

3.1. Implementation of SOTA algorithms 21

3.1.1. Simulated data characterisation 21

3.1.2. Testing and results 22

3.1.3. Discussion 22

3.2. Design of baseline correction method 23

3.3. RMSE on simulation with the designed algorithm.....29

4. Chapter 4. Algorithm evaluation **31**

4.1. Evaluation setup 31

4.2. Real data characterisation.....31

4.3. Results 33

4.4. Discussion 40

5. Chapter 5: Conclusions **42**

5.1. Summary 42

5.2. Conclusion.....42

5.3. Future work 44

Bibliography **45**

Abbreviations

^{1}H-MRS	Proton Magnetic Resonance Spectroscopy
ABfit	Adaptative Baseline fitting
AQoCE	Automated Quantitative approach based on a Convex Envelope
airPLS	adaptive iteratively reweighed Penalized Least Squares
BRCI	Baseline Recognition with Combination and Improvement
CSI	Chemical Shift Imaging
EPSI	Echo-planar Spectroscopic Imaging
FD	Frequency Domain
FFT	Fast Fourier Transform
FID	Free Induction Decay
FQN	Fit Quality Number
FT	Fourier Transform
MM	Macro Molecules
MRI	Magnetic Resonance Imaging
MRS	Magnetic Resonance Spectroscopy
MRSI	Magnetic Resonance Spectroscopy Imaging
NAA	N-acetylaspartate
NRM	Nuclear Magnetic Resonance
PRESS	Point Resolved Spectroscopy

ppm	parts per million
RF	Radio Frequency
SE	Spin Echo
SNR	Signal to Noise Ratio
SD	Standard Deviation
semiLASER	semi Localization by Adiabatic Selective Refocusing
SOTA	State Of The Art
STE	Stimulated Echo
STEAM	Stimulated Echo Acquisition Mode
SVS	Single Voxel Spectroscopy
T	Tesla
TARQUIN	Totally Automatic Robust Quantitation in NMR
TD	Time Domain
TE	Echo Time
TR	Repetition Time
VOI	Volume of Interest
WOS	Web of Science

List of Tables

Table 2.1. Baseline correction methods in the literature.....14

Table 2.2. Baseline correction methods in the literature.....18

Table 4.1. Description list of real data used for comparison part 2. 32

Table 4.2. FQN results of evaluating proposed method and state-of-the-art methods 39

Table 4.3. The average loss of Spectra 3 and 4 from our proposed method. 39

List of Figures

Figure 2.1. (A) FID example. (B) spectrum from FID after applying DFT [1]. 7

Figure 2.2. Short and long TE comparison for SVS spectrum acquired with a STEAM pulse sequence. (A) and (B) spectra were acquired using a magnetic field strength of 1.5 Tesla (T). (C) and (D) spectra were acquired using 3.0T. (E) spectrum was acquired using 7.0T, more commonly used for research purposes [1]. 9

Figure 2.3. 1H-MRS spectra before (blue) and after (red) residual water removal using a high-pass band-reject filter [7]. 10

Figure 2.4. Commonly observed artefacts in in vivo 1H-MRS spectra at short TE. A: 'smiley-artefacts' originated from non-ideal side effects of digital filtering, residual water components that were not completely suppressed, and MM components (e.g., mobile lipids and small/ medium-size peptides) producing broad lines in the spectrum. B: strong residual water affecting metabolites amplitudes. C: noticeable 'smiley-artefact'. 12

Figure 2.5. Mathematical models used for baseline correction in in vivo 1H-MRS and general NMR spectra. The middle layer shows mathematical approaches, and the outer layers show named algorithms. Marked algorithms are some of the methods that were tested in this thesis. Tables 2.1 and 2.2 contain a detailed list of the methods. 13

Figure 3.1. A: input signal (black) composed of artefact-free signal with simulated baseline (red). B: Spectral components of the input signal (black), simulated baseline (red), and artefact-free signal (blue). 21

Figure 3.2. RMSE between simulated baselines and estimated baselines by using ABfit, airPLS, BRCI, and CWT. A: RMSE from the 1,024 values of each signal. B: RMSE from 400 values in the metabolite section from 4.7048 ppm to 0.8825 ppm of each signal. The mean RMSE of the 500 estimated baselines is plotted as a red point.....23

Figure 3.3. Sections of an in vivo 1H-MRS spectrum. Sections A and C do not contain metabolite amplitudes, and section B contains metabolite amplitudes. 24

Figure 3.4. Pipeline of the proposed method. 25

Figure 3.5. Pre-estimated spectra for the proposed method. A: Spectrum1, from the moving mean filter in FD. B: Spectrum2, from truncation in TD. C: Spectrum3, from the minimisation step. D: Spectrum4, from the minimisation step. E: Spectrum5, mean between Spectra 2, 3, and 4.....26

Figure 3.6. Pre-estimated signals for the proposed method. A: Signal2, from truncation in TD. B: Signal3, from the minimisation step. C: Signal4, from the minimisation step. 27

(4.3).....28

Figure 3.7. Pipeline for determining the limits of each section of the spectrum. 29

Figure 3.8. RMSE between simulated and estimated baselines using ABfit, airPLS, BRCI, CWT, and our proposed algorithm. A: RMSE from the 1,024 values of each signal. B: RMSE from 400 values in the metabolite section from 4.7048 ppm to 0.8825 ppm of each signal. The mean RMSE of the 500 estimated baselines is plotted as a red point. 30

Figure 4.1. Evaluation setup for algorithms comparison. 31

Figure 4.2. Baseline estimations (red) and spectrum corrections (blue) for absorption channel of input spectrum n°1 (black) in dataset Generic12. Estimates made with (A) ABfit, (B) airPLS, (C) CWT, (D) BRCI, and (E) our method. 34

Figure 4.3. Baseline estimation (red) and spectrum corrections (blue) for absorption channel of input spectrum n°1 (black) in dataset Generic14. Estimations made with (A) ABfit, (B) airPLS, (C) CWT, (D) BRCI, and (E) our method. 35

Figure 4.4. Baseline estimation (red) and spectrum corrections (blue) for dispersion channel of input spectrum n°1 (black) in dataset Generic12. Estimations made with (A) ABfit, (B) airPLS, (C) CWT, (D) BRCI, and (E) our method. 36

Figure 4.5. Magnitude (Left) and Phase (Right) of the corrected spectrum (blue) for input spectrum n°1 (black) in dataset Generic12. Corrections were made with (A) ABfit, (B) airPLS, (C) CWT, (D) BRCI, and (E) our method. 36

Figure 4.6. FQN map displayed over CSI data (NAA-CH3 component) computed before baseline correction (Top-Left), and after correction with ABfit (Top-Right), airPLS (Middle-Left), BRCI (Middle-Right), CWT (Bottom-Left), and our method (Bottom-Right). Each colour map has a different range; the strongest red box in a map corresponds to the highest FQN obtained by that correction method, and the same for the strongest blue box. 37

Figure 4.7. FQN results for datasets Generic1 to Generic10. 38

Figure 4.8. Execution time in milliseconds (ms) of the implemented methods (ABfit, airPLS, BRCI, CWT, and Ours) for every signal corrected in all 14 datasets. Box plots are scaled in different ranges to show the different execution time boxes. A: scaled from 0ms to 36000ms. B: scaled from 0ms to 350ms. C: scaled from 0ms to 16ms. 38

1. Chapter 1. Introduction

1.1. Main introduction

Magnetic Resonance Spectroscopy (MRS) is a technique that provides a detailed fingerprint of the concentrations of major biochemical compounds present in biological tissues [1]. In comparison to Magnetic Resonance Imaging (MRI), where it is possible to identify anatomical structures in a volume of interest (VOI), biochemical analysis of living tissues also allow the determination of different types of tissues present in this volume, e.g. normal tissues or tumours. This technique can thus complement the diagnosis of diseases and sometimes provides greater specificity to define the correct medical diagnosis and treatment.

The support that MRS provides for disease diagnosis has been increasing over the last decades. Initially, researchers used this technique to identify biochemical composition in human organs, focusing mainly on tumours [2]. When observing anatomical images, determining the severity of a tumour in the brain and grading is a complicated task. After multiple investigations, researchers observed biochemical differences between normal and pathologic tissues, allowing doctors to make a more detailed diagnosis and thus act more appropriately to solve the problem [3]. In recent years, this technique has been refined and extended to multiple applications and different organs of the body, e.g., the prostate [4] and breast [5]. Despite all the advances, the technique is still not part of routine studies for disease diagnosis in non-academic centres due to the need to improve the quality of the spectrum before quantification.

In vivo MRS signals often have a low signal-to-noise ratio (SNR), and contain, apart from biochemical information of the metabolites, residual water and lipid signals. Because of this, good data acquisition is necessary to increase the SNR to distinguish the amplitudes of the different metabolites present in the brain [6]. Yet, in the case of proton MRS (^{1}H-MRS) of the brain, signals acquired for a short echo time (TE) present a strong baseline, which has negative effects on the accuracy with which the spectrum can be quantified [7].

There are multiple sources of disturbances that can contribute to the formation of a baseline. In some cases, applying frequency filters produces non-linear artefacts [8]. It is also possible that some

artefacts are produced by inhomogeneity of the magnetic field ($\vec{B}_0$) applied by the scanner [9]. Following this, it is possible to observe artefacts that may arise from residual water amplitudes or even lipids and other metabolites present in abundance in the brain [10]. Finally, some artefacts are produced simply by (involuntary) movements of the patient during the acquisition. These problems must be overcome, before quantifying the spectra, to obtain precise and reliable data, which allows, in its turn, a reliable diagnosis.

Over the last two decades, many algorithms have been proposed for estimating the baseline at in vivo ^{1}H-MRS — and general Nuclear Magnetic Resonance (NMR) — spectra. The most common approaches are smoothing filters and spline interpolations because, by definition, a baseline could be assimilated to a low-frequency signal with broad and smooth components. Other methods also include least squares, wavelets, Lorentzian functions, or even just computing the lower envelope of the spectrum. Algorithms like Adaptive Baseline fitting algorithm (ABfit) [11], Baseline Recognition with Combination and Improvement (BRCI) [12], Automated Quantitative approach based on a Convex Envelope (AQoCE) [13], and adaptive iteratively re-weighted Penalized Least Squares (airPLS) [14] propose semi-automatic functions, but the user requires expertise to identify the best entry values for a specific signal. Most methods work in the Frequency Domain (FD), but some of them, such as TARQUIN [15], also use Time-Domain (TD) information to estimate the baseline. There is no consensus on validating the performance of baseline correction algorithms. Some papers suggest determining the flexibility of the estimated spectrum to minimise quantification errors [16], while most works rely on visual inspection and comparison with past algorithms.

This thesis presents an extended review of significant artefacts found at *in vivo* ^{1}H-MRS signals and their causes. Experts' consensus and recommendations are also included [17]. In addition, this research introduces a detailed list of baseline correction algorithms for *in vivo* ^{1}H-MRS and general NMR spectra. This document proposes a novel method for improving baseline correction for *in vivo* ^{1}H-MRS signals by combining information obtained from TD and FD processing.

This document is structured as follows: Chapter 1 presents a brief introduction to the thesis, describes the thesis proposal, the aim of the project, general and specific objectives, the methodology for achieving the goals, and scopes and limitations. The state-of-the-art (SOTA) of

proton magnetic resonance spectroscopy are contained in Chapter 2, where we review the artefacts that affect these signals, their sources, and available methods for estimating the baseline components. We describe in Chapter 3 the implementation of the available SOTA algorithms found in the literary research; this chapter also contains the design of the proposed algorithm. All results of the final evaluation of the SOTA algorithms and our proposed algorithm are listed in Chapter 4. Finally, Chapter 5 summarises this thesis, the main conclusions, and thoughts for future steps.

1.2. Hypothesis

The baseline correction in brain ^{1}H-MRS spectra can be improved with respect to SOTA methods by the integration of time- and frequency-domain methods to the estimation algorithm .

1.3. Objectives

The main objective is to develop an algorithm for baseline correction of brain ^{1}H-MRS spectra by combining math approaches in Time Domain and Frequency Domain, to outperform the SOTA algorithms.

To achieve this goal, the following specific objectives were established:

1. Identify the most common and important artefacts in ^{1}H-MRS brain signals and available methods for baseline correction for ^{1}H-MRS spectra.

2. Design and implement a baseline correction algorithm aiming at improving the complex spectrum without overfitting the estimated baseline.

3. Evaluate the algorithm with simulated and real data, and compare it with state-of-the-art methods.

1.4. Methodology

1. Identify the most common and significant artefacts in ^{1}H-MRS brain signals.
    - Literature review about ^{1}H-MRS signal acquisition and preprocessing for short and long echo time.
    - Literature review about sources of baseline and their composition.

2. Identify available methods for baseline correction for ^{1}H-MRS and general NMR signals.
    - Literature review about available algorithms for baseline correction since 2005.
    - Literature review about mathematical methods implemented in baseline correction algorithms.
3. Determine the advantages and disadvantages of available methods for baseline correction.
    - Implement algorithms in MATLAB and RStudio for performance comparison.
    - Use simulated (ground truth) data for comparison between algorithms.
4. Design and implement the new baseline correction algorithm.
    - Design a new approach based on findings from previous steps.
    - Evaluate the approaches in MATLAB and RStudio using simulated (ground truth) data, i.e. real signals with minimum baseline effects that will be combined with simulated (already known) baselines.
    - Select the best algorithm based on the minor alteration of the metabolite peaks, magnitude and phase.
5. Evaluate and compare the proposed algorithm.
    - Evaluate the approach using real anonymised *in vivo* ^{1}H-MRS signals for short TE.
    - Evaluate the approach by using the Fit Quality Number (FQN).
    - Compare the results from the proposed algorithm and the available state-of-the-art algorithms by using FQN.
6. Improvements after evaluation.
    - Identify potential problems and improvements for the proposed algorithm, and implement corrections.
    - Identify the advantages and disadvantages of the proposed algorithm compared with the available approaches.
7. Writing the WOS article and final thesis report.

- Writing a WOS article describing the developed method, to be submitted to Magnetic Resonance Imaging or NMR in Biomedicine journal.
- Writing the final thesis report.

1.5. Scope and limitations

As mentioned in the methodology, the literature review about existing baseline correction algorithms will comprehend only the approaches published since 2005. This assumption is based on the idea that every past algorithm has already been studied, analysed, implemented, refuted, or improved by a recent publication. Although algorithms proposed before 2005 will be included in the review but not implemented or evaluated in the following steps of this thesis.

Regardless of the programming language in which each algorithm has been coded, the implementation and evaluation of each method, including the proposed one, will be performed in MATLAB and RStudio. This statement relies on the efficiency optimisation of the execution time by using only these programming tools for the entire thesis.

Every data used in this project must be real or simulated from real data to be used for scientific purposes. Therefore, the data will be entirely and meticulously anonymised to protect patient privacy. The data already anonymised will be provided by Ph.D. Johannes Slotboom from the University Hospital of Bern, Switzerland.

2. Chapter 2. State of the Art

2.1. Magnetic resonance spectroscopy

Magnetic Resonance Spectroscopy (MRS) and MRS Imaging (MRSI) are non-invasive techniques for obtaining *in vivo* information on the biochemical processes inside the human body [18]. MRI, MRS, and MRSI are often applied together in one examination. The technique begins with NMR signals being acquired by the scanner in TD, followed by the conversion of the signals to FD spectra. Preprocessing is often applied to correct severe imperfections and artefacts such as phase, baseline signals, and residual water amplitudes. Preprocessing the signals is strictly necessary before the quantification step, where metabolite peaks in the spectra are identified, and values are assigned according to their amplitude. Only afterwards, clinicians analyse the results.

Proton MRS (^{1}H-MRS) is based on NMR principles. In simple terms, a magnetic field ($\vec{B}_0$) is used to bring atoms (whose nuclei have a magnetic momentum) within the human body to the Boltzmann distribution [19]. Subsequently, a radio frequency (RF) pulse is emitted to a specific atom — hydrogen protons in the case of signals used in this thesis — transferring coherence to the spin system [20]. To change the state of these atoms, an RF pulse must be applied at the resonance frequency of the selected atom under the influence of the magnetic field by using the Larmor equation [1]. After the stimulation, the atoms release the accumulated energy to return to the Boltzmann distribution. Finally, this energy is captured by the magnetic resonator or RF-coil as signals in the time domain, also known as free induction decay (FIDs), as the signal shown in Figure 2.1.A.

Signals from protons or other elements nuclei (e.g., phosphorus or sodium) can be acquired in an NMR study. However, MRS measures biochemical components (i.e., significant metabolites inside the human body). The Chemical Shift phenomenon is considered to differentiate each metabolite peak in the spectrum [21]. In simple words, the resonance frequency varies minimally depending on the atoms that compose a molecule, apart from the element being measured, as a result of a local magnetic field surrounding each molecule. The Chemical Shift is measured in parts per million (ppm). The resonance frequency of each molecule in ppm has already been standardised [1]. An

example of the spectrum after applying the Discrete Fourier Transform (DFT) to an FID is shown in Figure 2.1.B, including the expected peaks from each molecule to be identified.

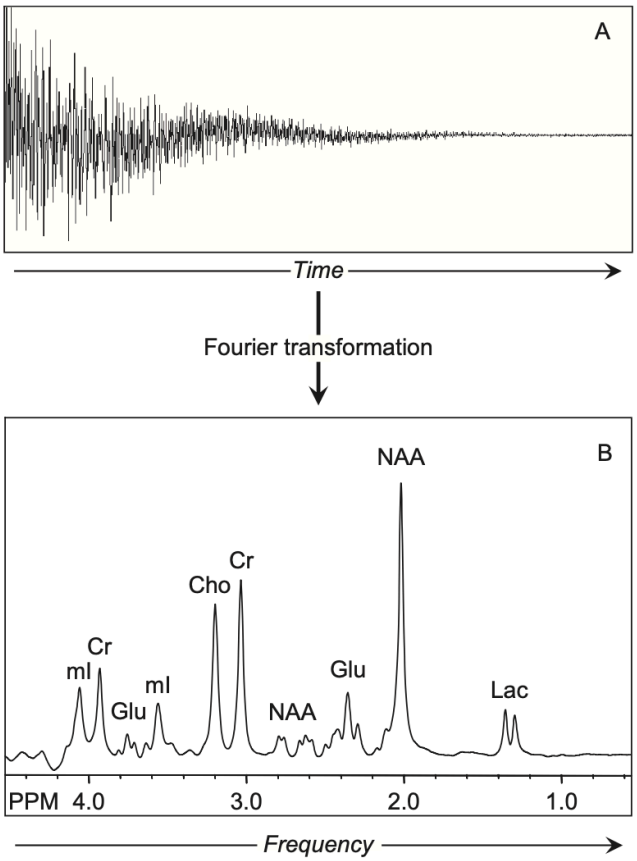

Figure 2.1. (A) FID example. (B) spectrum from FID after applying DFT [1].

2.2. Signal acquisition and preprocessing

MRS studies can be performed in two major modalities: Single-Voxel Spectroscopy (SVS) (where signals are acquired from a single region), and Multi-Voxel Spectroscopy, also known simply as MRSI or Chemical Shift Imaging (CSI) (where signals are simultaneously acquired from multiple regions) [22]. In SVS studies, three RF pulses are emitted to a VOI to receive signals orientated in three orthogonal axes. The most common pulse sequences are PRESS (three pulses in 90º-180º-180º) and STEAM (three pulses in 90º-90º-90º). Applying these pulse sequences improves the spatial localisation of the signal but often decreases the SNR due to pulse imperfections [23]. Other techniques, such as semi-LASER (Localization by Adiabatic Selective Refocusing) and EPSI

(Echo-planar Spectroscopic Imaging), can be found in [24]. PRESS and STEAM sequences can also be used in MRSI. Still, other sequences, such as EPSI, are also implemented to improve acquisition quality because of the bigger VOI and smaller regions (i.e., divisions) than in SVS studies. It is important to mention that FIDs are generated after the first pulse, and the second and third pulses create spin-echoes (SE) and stimulated echoes (STE) [25].

Timing is important when acquiring signals, and in MRS — just like in NMR — relaxation times must be considered while planning a pulse sequence. The relaxation times T_1 and T_2, known as longitudinal and transverse relaxation times, are both natural constants, and the timing of the study must be adapted to them. The repetition time (TR) is the total time the sequence takes to complete, and it is then repeated. A complete recovery of the atoms into the Boltzmann distribution is needed to perform a new sequence. Usually, TR is considered as five times T_1 or higher. The echo time (TE) is the response time from the middle of the first RF pulse until the peak of the echo [22]. Depending on the length of the TE, the acquisition can be for short TE (~20ms) or long TE (~140ms). An adequate TE is essential to observe signals from every important metabolite on each acquisition, and to reduce the noise produced by big molecules (e.g. lipids) [1]. In Figure 2.2, an SVS spectrum obtained after applying a STEAM sequence shows the different outcomes depending on the TE used. For short TE, the spectrum amplitudes are higher than for long TE. In addition, more metabolite peaks are observed in the short TE spectrum, but lipid and lactate amplitudes also emerge [1].

FIDs are time-domain signals that need to be transformed into frequency-domain to analyse the concentrations of the metabolites in the VOI. One FID can be mathematically represented as a complex exponential decay oscillator. In the following equation, the frequency is represented with Ω, the initial amplitude A_0, the initial phase offset ϕ_0, and the decaying factor λ, i denotes the imaginary component, and t is the time vector [7]:

$$f(t) = A_0 e^{i\Omega t - \lambda t - i\phi_0} \tag{2.1}$$

After transforming the FIDs into the frequency domain, the spectrum is compounded by a real part (also called absorption spectrum) and an imaginary part (called dispersion spectrum). Both the pre-processing of the signal and the analysis of the concentrations of the metabolites must be performed using the absorption and dispersion spectra.

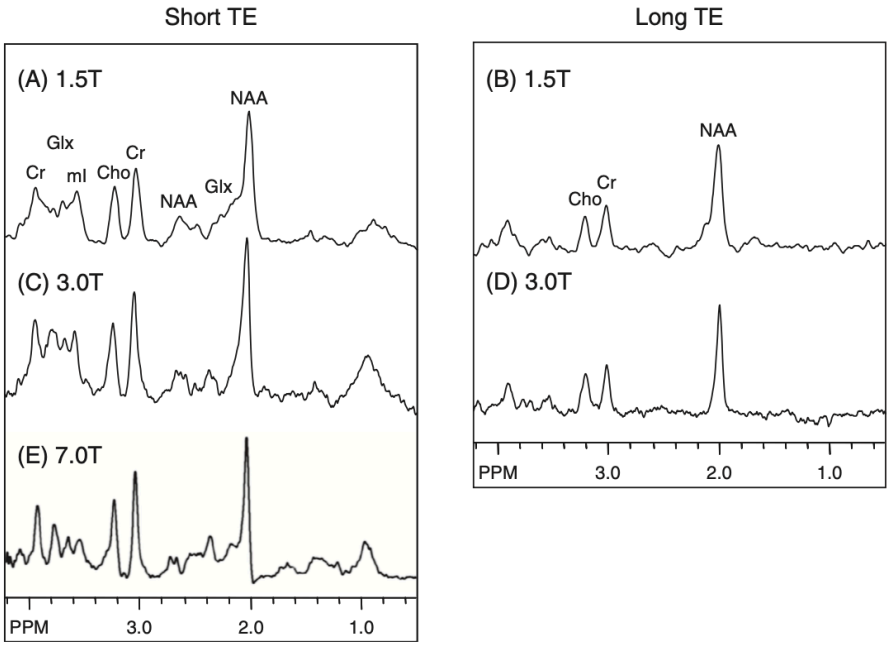

Figure 2.2. Short and long TE comparison for SVS spectrum acquired with a STEAM pulse sequence. (A) and (B) spectra were acquired using a magnetic field strength of 1.5 Tesla (T). (C) and (D) spectra were acquired using 3.0T. (E) spectrum was acquired using 7.0T, more commonly used for research purposes [1].

The data can be pre-processed in the time and/or frequency domain to increase the FD SNR, but reducing the spectral resolution. For example, a method for reducing the FD noise in the signal is multiplying by a decreasing function. Also, it is common to convert the Lorentzian line shape of the spectrum into a Gaussian line shape by applying a Lorentzian-Gaussian Transform [7]. A mandatory pre-processing is the suppression of water and macromolecular (MM) components (e.g., lipids) and residual water removal. Because the amplitude of the water in the spectrum is larger than the amplitude of other small molecules (e.g., metabolites like N-Acetylaspartate (NAA)), suppressing and removal of the water signal is important to proceed with the study of the metabolites peaks. In Figure 2.3, a spectrum without residual water suppression is presented in contrast to the spectrum after residual water suppression [7].

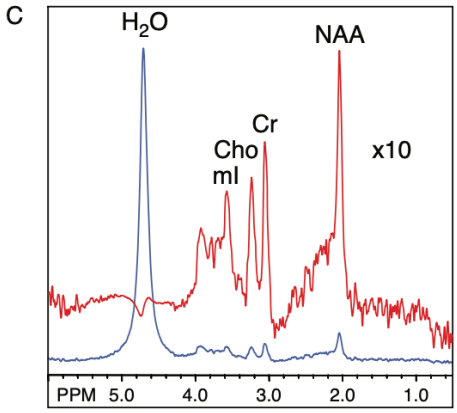

Figure 2.3. ^{1}H-MRS spectra before (blue) and after (red) residual water removal using a high-pass band-reject filter [7].

2.3. Artefacts in *in vivo* ^{1}H-MRS spectra and characterisation of baseline.

As many experts remark, the term baseline should be used exclusively for the smoothly varying signal underlying the metabolite spectra [26]. This is commonly mistaken by including MM components (e.g., proteins, lipids) when they should be considered as MM background signals. Their differences rely on their sources and the methods to correct the irregularities that arise from both signals. Background signals commonly appear in short TE as broad spectral lines overlapping in the frequency domain with the metabolites components [27]. These signals are usually eliminated with a fitting model before the acquisition, estimating the MM components and then subtracting the signal from the acquired data [28, 29]. Also, some researchers have found that the effects of these signals can be minimised by using a long TE [30]. Unfortunately, even after applying fitting models or adjusting parameters, some MM still appear in the spectrum. Bertholdo et al. [6] described most metabolites and MM that can be observed in ^{1}H-MRS, e.g., lipids and lactate that remain after the MM fitting. But, lipids are not visible in long TE spectra, while lactate appears in short and long TE spectra, and its peak is inverted for TE between 135 and 144 ms.

Baseline sources are more numerous and difficult to estimate. Even after MM contributions are modeled and corrected prior to metabolite fitting, baseline signals still appear from any unexpected signal sources (e.g., from the broad tails of imperfect suppressed water peak) [17]. Tang [8] concluded that for general NMR spectra (i.e., not only *in vivo*), major sources of baseline artefact also arise during the acquisition due to inappropriate sampling time, or they produce by filtering the

signals. Most of these problems can easily be overcome before and during the acquisition, and the remaining components must be corrected during data pre-processing. For *in vivo* ^{1}H-MRS, Kreis et al. [26] concurred with sources from analogue and digital filtering affecting the initial points of the FID.

Furthermore, a detailed list of sources for baseline artefacts is presented, including (1) mostly originated from sub-optimal localisation performance, (2) non-reproducible features caused by water and/or mobile lipids from outside the VOI, (3) insufficient water suppression, (4) hardware imperfections affecting the first data points in the FID, and (5) inaccurate timing of the echo during data acquisition. Some observable effects in the spectrum are indicated in Figure 2.4. For artefacts from source (2), Posse et al. [10] explain that some baseline artefacts are originated from some signals that spread from the peripheral fat layer in the scalp located at the interface of two adjacent voxels.

Kreis et al. [26] classify baseline correction as an operation for removing imperfections. Furthermore, in [31], the author states that a wrong baseline model could be a source of systemic errors. However, knowing baseline signals could be useful for checking: (1) ghosts, i.e., spurious echoes originated due to inhomogeneities in the magnetic field, (2) unidentified metabolites, (3) outer volume signals, (4) wrong metabolite peaks assignments, and (5) standard deviation (SD) of residual signals and noise.

2.4. Baseline correction for *in vivo* ^{1}H-MRS and general NMR spectra

The unwanted features exposed in the last section are almost impossible to predict and to recreate prior data acquisition. Near et al. [17] suggest that when handling baseline artefacts, either time-domain or frequency-domain methods could be used, assuming a rapid decay of baseline signal components (i.e. components appear at initial points of the FID) and smooth line shape of the spectral baseline. Kreis et al. argue that most baseline correction approaches have a mathematical base, usually without physical meaning, e.g., splines [32] and wavelets [33] that represent the broad features of the baseline or simply considering the initial part of the FID [34]. Nevertheless, implementing a good and reliable baseline correction algorithm is necessary to perform adequate data quantification.

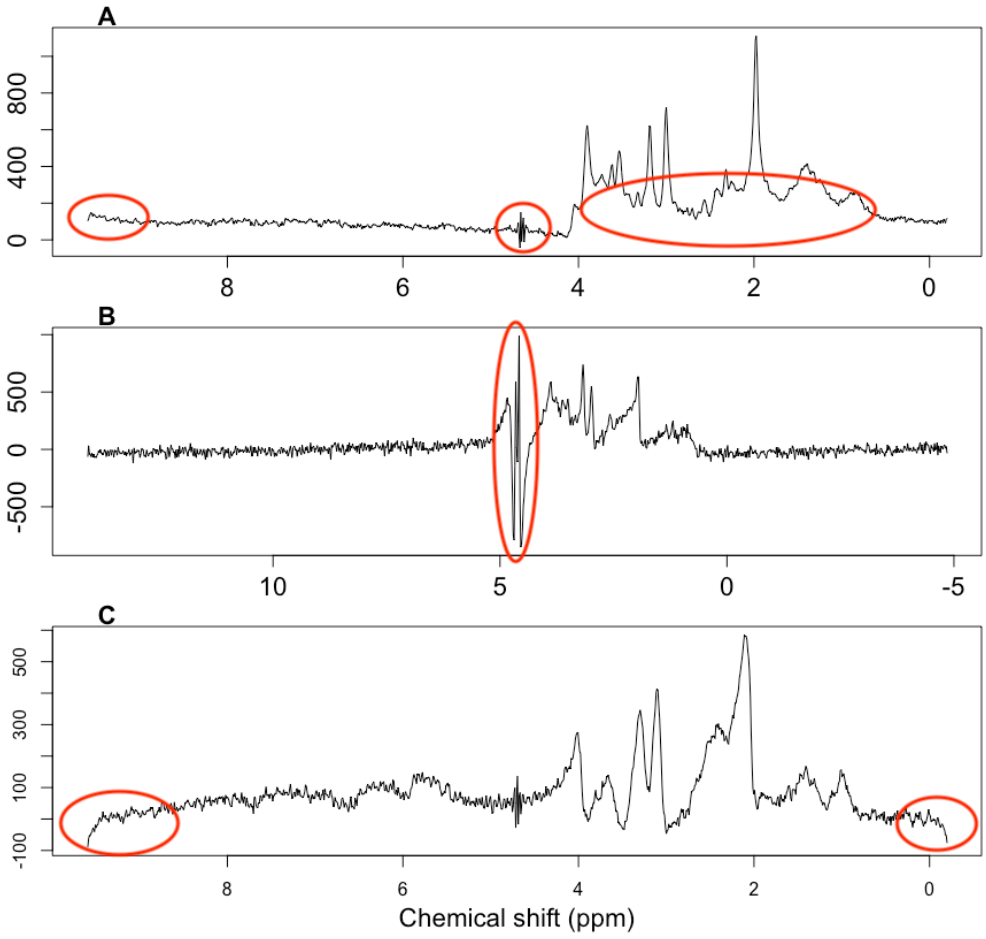

Figure 2.4. Commonly observed artefacts in *in vivo* ^{1}H-MRS spectra at short TE. **A:** 'smiley-artefacts' originated from non-ideal side effects of digital filtering, residual water components that were not completely suppressed, and MM components (e.g., mobile lipids and small/medium-size peptides) producing broad lines in the spectrum. **B:** strong residual water affecting metabolites amplitudes. **C:** noticeable 'smiley-artefact'.

Most algorithms approach baseline removal in the frequency domain. For simplification, the spectrum is commonly treated as a signal, and the object is to find its lower frequency components. Polynomial fitting was one of the initial methods used to estimate baselines, combined with a parametrized-automatic algorithm for determining points that are most likely to match with a smooth baseline definition, such as the methods proposed by Dietrich et al. [35] (derivation plus polynomial fitting) and later Brown [36] (iteration method with Bernstein polynomials) to correct spectral baselines in NMR spectra. Young et al. [33] proposed one of the first baseline correction algorithms for *in vivo* ^{1}H-MRS spectra with short TE, based on a least square model of the prior

knowledge of MM components to eliminate background signals, followed by a smoothing filter and wavelet transform to estimate the nuisance spectral components. In subsequent research, wavelets have been frequently used. For example, Golotvin et al. [37] and Chang et al. [38], employed average filters to estimate the baseline in NMR spectra. The program TARQUIN [15] uses a 100-point Gaussian window convolution to correct short TE *in vivo* ^{1}H-MRS baseline. Figure 2.5 shows a diagram with every mathematical method found during this review.

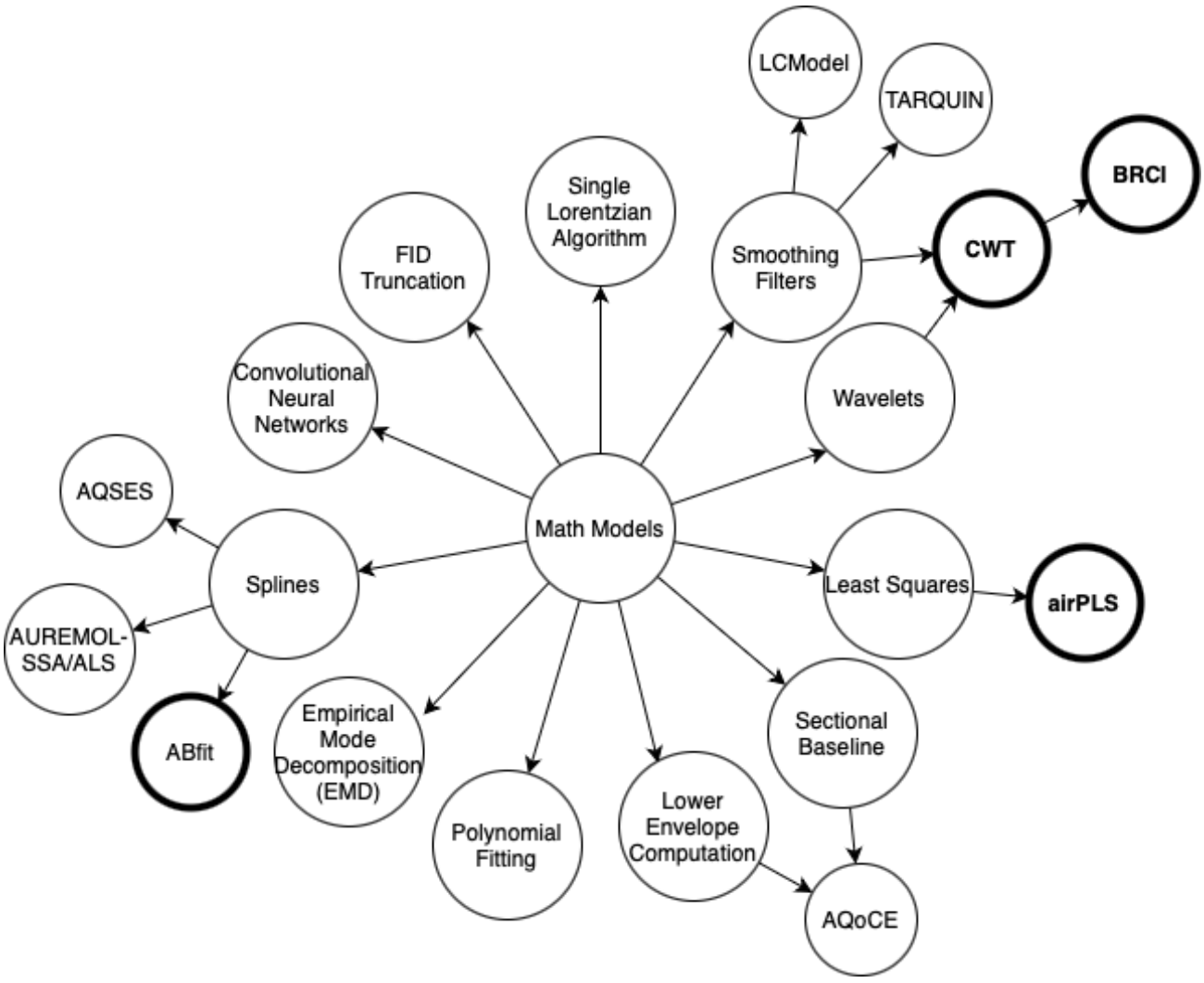

Figure 2.5. Mathematical models used for baseline correction in *in vivo* ^{1}H-MRS and general NMR spectra. The middle layer shows mathematical approaches, and the outer layers show named algorithms. Marked algorithms are some of the methods that were tested in this thesis. Tables 2.1 and 2.2 contain a detailed list of the methods.

The most common FD approaches are smoothing filters and spline interpolation. Widely used quantification algorithms like LCModel [39] and AQSES [40] include smoothing and penalised splines for baseline correction. A more recent algorithm, ABfit [11], uses penalised splines to achieve optimal flexibility of the baseline spectrum. By contrast, algorithms in the time domain have been largely used, and in the last three decades, only two approaches have been partially proposed. AQSES includes TD filtering by using an FIR filter for removing specific resonances. Ratiney et al. [34] implemented a quantification algorithm omitting baseline components by truncating the initial points of the FID.

In Tables 2.1 and 2.2 a detailed list is presented with every baseline correction algorithm for *in vivo* ^{1}H-MRS and general NMR that was found in this review. A total of 20 documents that propose a method for baseline estimation were found, including articles, communications and conference papers. Only baseline correction methods were presented in 12 papers, and others were included in the remaining documents as a sub-step for a quantification algorithm. Also, 12 methods were designed for removing in *in vivo* ^{1}H-MRS spectra, and almost all of them for short TE. Most algorithms can handle complex spectra [41-44], and a few were developed for handling only the absorption component [39, 45, 46].

Table 2.1. Baseline correction methods in the literature.

Author	DOI	Short name	Aim	Type of spectra	TE
W. Dietrich et al. Pub. year 1991	doi.org/ 10.1016/0022-2364(91)90402-F	Not found	Baseline correction	NMR spectra	Not mentioned
D. E. Brown Pub. year 1995	doi.org/ 10.1006/ jmra.1995.1138	Not found	Baseline correction	NMR spectra	Not mentioned
K. Young et al. Pub. year 1998	doi.org/ 10.1002/ mrm.1910400606	Not found	Background signals with baseline correction	*In vivo* ^{1}H-MRS	Short
S. Golotvin Pub. year 2000	doi.org/ 10.1006/ jmre.2000.2121	Not found	Baseline correction	NMR spectra	Not mentioned

S. W. Provencher Pub. year 2001	doi.org/ 10.1002/ mrm.1910300604	LCModel	Quantification algorithm with baseline correction	*In vivo* ^{1}H-MRS	Both
H. Ratiney et al. Pub. year 2004	doi.org/ 10.1007/ s10334-004-0037-9	Not found	Quantification algorithm with baseline correction	*In vivo* ^{1}H-MRS	Short
J. C. Cobas et al. Pub. year 2006	doi.org/ 10.1016/ j.jmr.2006.07.013	Not found	Baseline correction	NMR spectra	Not mentioned
P. Gillies et al. Pub. year 2006	doi.org/ 10.1002/ nbm.1060	Not found	Quantification algorithm with baseline correction	*In vivo* ^{1}H-MRS	Long
D. Chang et al. Pub. year 2007	doi.org/ 10.1016/ j.jmr.2007.05.008	Not found	Baseline correction	NMR spectra	Not mentioned
J. Poullet et al. Pub. year 2007	doi.org/ 10.1002/ nbm.1112	AQSES	Quantification algorithm with baseline correction	*In vivo* ^{1}H-MRS	Short
Z. Zhang et al. Pub. year 2010	doi.org/ 10.1039/ b922045c	airPLS	Baseline correction	NMR spectra	Not mentioned
M. Wilson et al. Pub. year 2011	doi.org/ 10.1002/ mrm.22579	TARQUIN	Quantification algorithm with baseline correction	*In vivo* ^{1}H-MRS	Short
S. De Sanctis et al. Pub. year 2011	doi.org/ 10.1016/ j.jmr.2011.03.001	AUREMOL-SSA/ALS	Background signals with baseline correction	NMR spectra	Not mentioned
Q. Bao et al. Pub. year 2012	doi.org/ 10.1016/ j.jmr.2012.03.010	BRCI	Baseline correction	NMR spectra	Not mentioned
A. J. Wright et al. Pub. year 2012	doi.org/ 10.1002/ mrm.24182	Not found	Baseline correction	*In vivo* ^{1}H-MRS	Long

M. A. Parto et al. Pub. year 2014	doi.org/ 10.1109/ EMBC.2014.6 944302	Not found	Baseline correction	*In vivo* ^{1}H-MRS	Short
W. Dou Pub. year 2015	doi.org/ 10.1371/ journal.pone.01 37850	AQoCE	Quantification algorithm with baseline correction	*In vivo* ^{1}H-MRS	Short
O. Bazgir Pub. year 2018	doi.org/ 10.1109/ ssiai.2018.8470 319	Not found	Baseline correction	*In vivo* ^{1}H-MRS	Short
H. Hun Lee et al. Pub. year 2017	doi.org/ 10.1002/ mrm.26502	Not found	Quantification algorithm with baseline correction	*In vivo* ^{1}H-MRS	Short
M. Wilson Pub. year 2021	doi.org/ 10.1002/ mrm.28385	ABfit	Baseline correction	*In vivo* ^{1}H-MRS	Short

Observation: This first part presents every baseline correction method found from 1990 to 2021. Only methods that propose a new approach were included in the list, even if the algorithm was proposed as a step of another algorithm (e.g. quantification). This first part shows the following categories: (1) DOI, (2) the short or commercial name of the general proposed algorithm, (3) the aim of the presented work, (4) if the algorithm was proposed for general NMR spectra or specifically for *in vivo* ^{1}H-MRS, and (5) if the algorithm was proposed/tested for short or long (or both) TE.

2.5. Validation and comparison methods

Most of the algorithms presented in the previous sub-section were tested with simulated and real data. In some cases, they are compared with other methods for performance and visual examination. In any case, no possible testing approach has been found to establish the efficiency in baseline correction. Zhang et al. [16] suggest that a method for baseline smoothness and flexibility degree computation, based on root-mean-square error (RMSE), can be used to determine the best baseline to fit, i.e., under- or over-smoothed baseline could lead to significant quantification errors.

The RMSE between two signals is used in this project for evaluating the performance of the selected state-of-the-art algorithms. We compute the RMSE between two list of N values (simulated baseline S and estimated baseline $\hat{S}$) with equation (2.2).

$$RMSE = \sqrt{\frac{\sum_{i=1}^{N} (S_i - \hat{S}_i)^2}{N}} \tag{2.2}$$

Slotboom et al. [47] presented Fit Quality Number (FQN), a value for determining the quality of model fitting after quantification. FQN is the ratio between the signal model (i.e., model after quantification) and the fit residuals (i.e., signal model minus experimental signals). For FQN values higher than 1.0, the model does not completely match the initially acquired signal, meaning that the model has been negatively over-modified. The same situation happens for FQN values lower than 1.0, where the model is over-fitted, i.e., artefacts were overestimated. The model has a perfect match on average with the experimental signal when FQN is equal to 1.0. Poor FQN results suggest problems in any of the pre-processing steps, e.g., insufficient water removal, poor MM components model, or poorly described baseline, resulting in an inadequate signal model. The FQN is calculated with equation (2.3), with Q_{fit} representing the FQN, σ is the variance of the signal noise component, R is the residue from the quantification process, and N is the number of points of the least-squares fit.

$$Q_{fit}(N) = \frac{R}{N \cdot \sigma} \tag{2.3}$$

Alternatively, the FQN can be calculated only for the absorption channel using equation (2.4), where $Q_{fit-abs}$ is the FQN of the absorption channel, σ_{res} is the variance of the signal noise component, and σ_{res} is the variance of the residue from the quantification process.

$$Q_{fit-abs}(N) = \frac{\sigma_{res}}{\sigma_{noise}} \tag{2.4}$$

Table 2.2. Baseline correction methods in the literature.

Author	Availability	Signal	Domain	Automatic	Math method
W. Dietrich et al.	Not found	N.M.	FD	Automatic Parametrized	Derivation, and polynomial fitting
D. E. Brown	Not found	N.M.	FD	Automatic Parametrized	Iteration, and Bernstein Polynomials
K. Young et al.	Not found	N.M.	FD	Automatic Parametrized	Least squares with prior knowledge for model fitting, and wavelets
S. Golotvin	Not found	N.M.	FD	Automatic Parametrized	Standard deviation plus threshold for point detection, and average smoothing filter
S. W. Provencher	Java-based, software package	Abs	FD	Automatic Parametrized	Regularization method, and smoothing splines
H. Ratiney et al.	Not found	Clx	TD	Automatic Parametrized	Truncation of the first 3 points
J. C. Cobas et al.	MATLAB	Abs	FD	Automatic Parametrized	Continuous wavelet transformation, and whittaker smoother algorithm
P. Gillies et al.	Not found	Clx	FD	Automatic Parametrized	The DAUB4 discrete wavelet transform
D. Chang et al.	Not found	N.M.	FD	Automatic Parametrized	Smoothing filters
J. Poullet et al.	Java-based, software package	Clx	TD	Parametrized	FIR filter for specific resonances, and penalized splines
Z. Zhang et al.	R, MATLAB, Python, C++	Clx	FD	Parametrized	Least squares
M. Wilson et al.	Software package	Clx	FD	Automatic Parametrized	Smoothing filter with 100 points Gaussian window convolution, and linear extrapolation
S. De Sanctis et al.	Software package	Clx	FD	Automatic Parametrized	Linear spline interpolation
Q. Bao et al.	MATLAB	Abs	FD	Automatic Parametrized	Continuous wavelet transformation, Whittaker smoother algorithm, sliding window algorithm, and iterative threshold algorithm
A. J. Wright et al.	Not found	Clx	FD	Automatic Parametrized	Single lorentzian algorithm

M. A. Parto et al.	Not found	Clx	FD	Automatic Parametrized	Empirical Mode Decomposition
W. Dou	Not found	N.M.	FD	Automatic Parametrized	Lower Convex Envelope (convex hull), and sectional baseline removal
O. Bazgir	MATLAB	Abs	FD	Automatic Parametrized	Local minima polynomial interpolation
H. Hun Lee et al.	Not found	Clx	FD	Automatic Parametrized	Convolutional Neural Network with training model
M. Wilson	R	Abs	FD	Automatic Parametrized	Penalized splines (P-splines) smoothing.

Observation: This second part shows the following categories: (1) the programming language the method was written or if the algorithm can be found as a software package, (2) if the algorithm was proposed for address complex (Clx) signals or only absorption (Abs)/dispersion(Dsp) components, Not Mentioned (N.M.), (3) if the work proposes a time domain or frequency domain approach (or both), (4) if the algorithm is fully automatic, semi-automatic (parameters can be set), or it requires entry values, and (5) the main implemented mathematical methods.

2.6. Discussion

This chapter presented a review of *in vivo* ^{1}H-MRS and its relevance for early disease diagnosis. As shown, these signals are commonly affected by a variety of noisy components coming from different sources, e.g., bad $\vec{B}_0$ shimming, digital filters, patient involuntary movement, etc. Most of these sources can be overcome by optimizing acquisition procedures, followed by applying correction algorithms for water and other MM components. However, some components still appear after these corrections, and their source remains unknown or complex to address by conventional approaches. Therefore, an algorithm for baseline estimation is needed.

Many algorithms for baseline correction have been proposed in the last two decades. Most of these algorithms work in FD since it is very intuitive, and the corrected spectrum can be visually examined. But, only a few methods use the whole complex signal, which is crucial when the quantification step requires both the absorption and dispersion channels. Also, a disadvantage of most SOTA algorithms lies in their exclusive reliance on mathematical formulations, rather than a comprehensive physical interpretation. Their emphasis is predominantly centered on improving the visual appearance of the spectrum instead of finding the baseline components to minimise the bias in parameter estimates.

Another very important feature to take into consideration is the full automatisation of the algorithm. Almost every SOTA algorithm that surpasses the problems mentioned above requires entry parameters, therefore, whoever uses the algorithms must have experience in *in vivo* ^{1}H-MRS signals, baseline signals, and the baseline estimation algorithm to perform an adequate correction. If the person who runs the study does not have the necessary expertise using the algorithm, then it might take longer than to perform the standard process for baseline correction, i.e., interpolate manually picked points of the spectrum, which also requires a high level of experience. Also lactate could potentially be a problem for baseline correction algorithms because its peak is inverted for TE between 135 and 144 ms.

Addressing the baseline correction problem in the time domain could improve the output because sections of the signal directly affected by baseline sources would be incorporated into the result. Finally, a new algorithm should only have the raw signal as input, or a minimum number of entry parameters to be set/defined by the user, to speed up the pre-processing of the signal.

3. Chapter 3. Testing SOTA algorithms and design of the proposed algorithm

3.1. Implementation of SOTA algorithms

3.1.1. Simulated data characterisation

The dataset used for testing the algorithms was composed of 500 complex signals of 1,024 values each, which were pre-processed using removing most amplitudes from water and MM, which encompassed Fourier transformation, frequency alignment of the spectra, and automatic zero-order phasing, to obtain an artefact-free spectrum. Then, an equal number of different baseline signals were simulated by using equation (2.1), considering that baselines decay rapidly and only affect the first points of the acquired signals. An example of these signals and baselines is shown in Figure 3.1; both were added together to obtain the inputs for the algorithms.

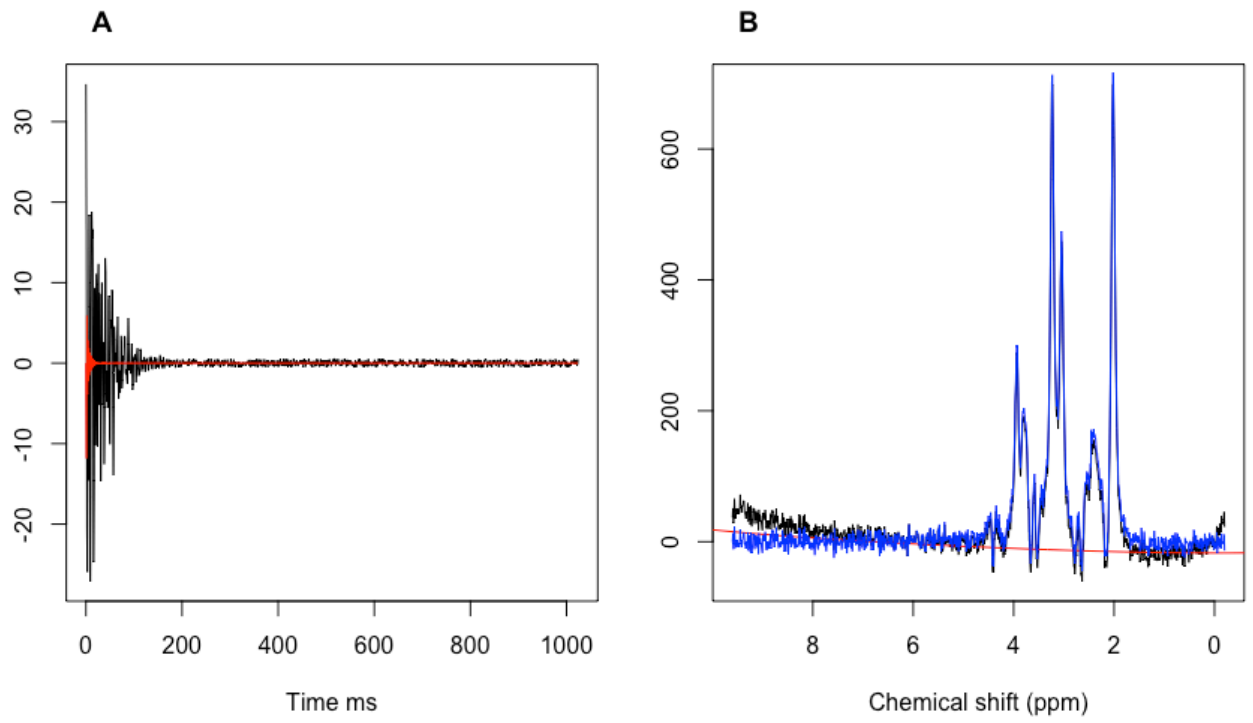

Figure 3.1. A: input signal (black) composed of artefact-free signal with simulated baseline (red). **B**: Spectral components of the input signal (black), simulated baseline (red), and artefact-free signal (blue).

3.1.2. Testing and results

Four algorithms were found to meet the conditions proposed in the previous section: (1) adaptive iteratively re-weighted penalised least squares (airPLS) by Zhang et al. [14], (2) a method based on Continuous Wavelet Transformation and Whittaker Smoother algorithm by Cobas et al. [45], named CWT for the purposes of this thesis, (3) Baseline Recognition with Combination and Improvement (BRCI) by Q. Bao et al. [12], and (4) Adaptative Baseline fitting (ABfit) by M. Wilson [11]. These algorithms were downloaded from the repositories indicated by their authors. For the implementation, MATLAB R2021a and RStudio v1.4.1717 were used in a Mac mini (M1, 2020) with 16GB RAM.

The baselines estimated with the four SOTA algorithms were compared to the original simulated baselines, using the RMSE equation (2.2) to determine the difference in (1) the 1,024 values of each signal and (2) the metabolite range considering the values from 4.7048 ppm to 0.8825 ppm (400 values in total). The results are presented in Figure 3.2. On average, CWT had the lowest RMSE for the whole signal, around 42.21, followed by BRCI with 60.35, then ABfit with 140.85, and airPLS with 142.33.

3.1.3. Discussion

In total, 16 algorithms found in the literature were discarded, most of them because they were not available at the time of this study. Some baseline correction algorithms were proposed as a sub-step for a quantification algorithm, we discarded these algotihms because we needed to use directly the baseline correction algorithm into our evaluation pipeline.

From the implementation of the algorithms that met the requirements (airPLS, CWT, BRCI, and ABfit), the RMSE values in Figure 3.2 show that the main problem relies on the metabolite section of the spectrum, being the RMSE values in the metabolite section always higher for the whole spectrum. The worst RMSE results were obtained by ABfit, followed closely by airPLS, but it is important to notice that the airPLS method is the only one tested that works for both absorption and dispersion channels. Also, airPLS claims that the result can be improved by setting new parameters, but that requires more knowledge of the algorithm.

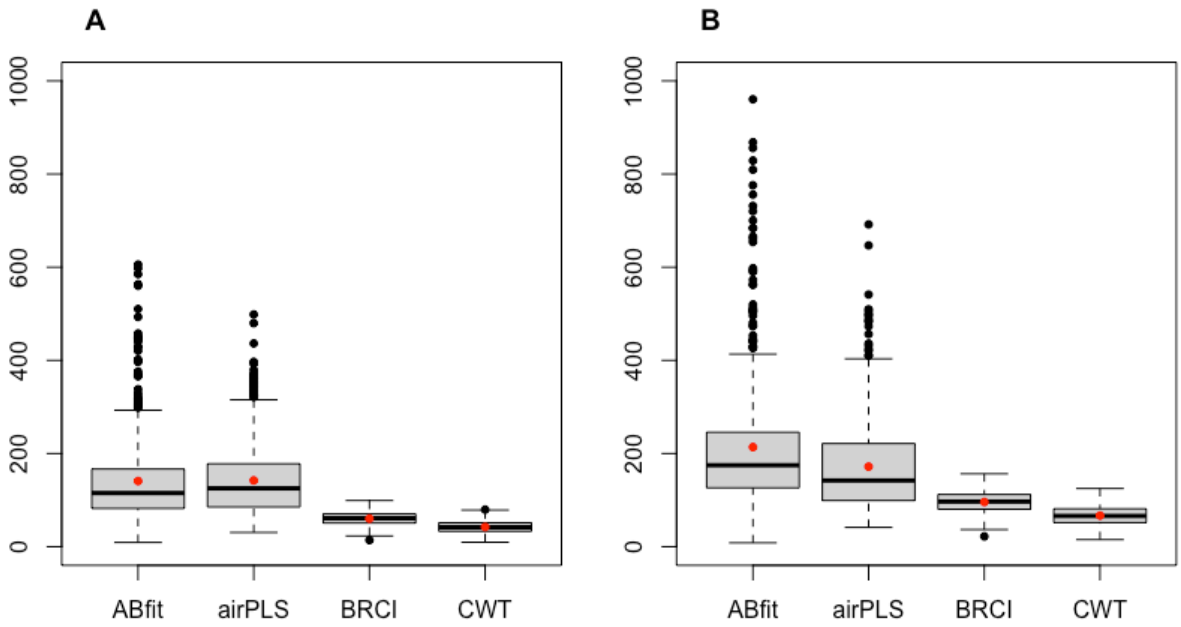

Figure 3.2. RMSE between simulated baselines and estimated baselines by using ABfit, airPLS, BRCI, and CWT. **A**: RMSE from the 1,024 values of each signal. **B**: RMSE from 400 values in the metabolite section from 4.7048 ppm to 0.8825 ppm of each signal. The mean RMSE of the 500 estimated baselines is plotted as a red point.

During the testing of the available methods, it was possible to notice that, although most algorithms performed poorly for the ground truth data, they still can be improved, mainly because they return acceptable values in sections of the spectrum without metabolites.

3.2. Design of baseline correction method

To address the poor correction in the metabolites ppm range, the spectrum was divided into three sections, as indicated in Figure 3.3. Sections A and C correspond to frequencies without metabolite amplitudes. Baseline components are very notorious in these sections, and they can be easily corrected by applying a smoothing filter in FD. However, as discussed previously, most algorithms have problems to estimate the baseline signal at the metabolite amplitudes, which corresponds to section B.

The diagram in Figure 3.4 presents the final version of the proposed method for estimating the baseline. The input is a time-domain in vivo ^{1}H-MRS signal, and the output is the estimated baseline, which is built up from four pre-estimated spectra as follows:

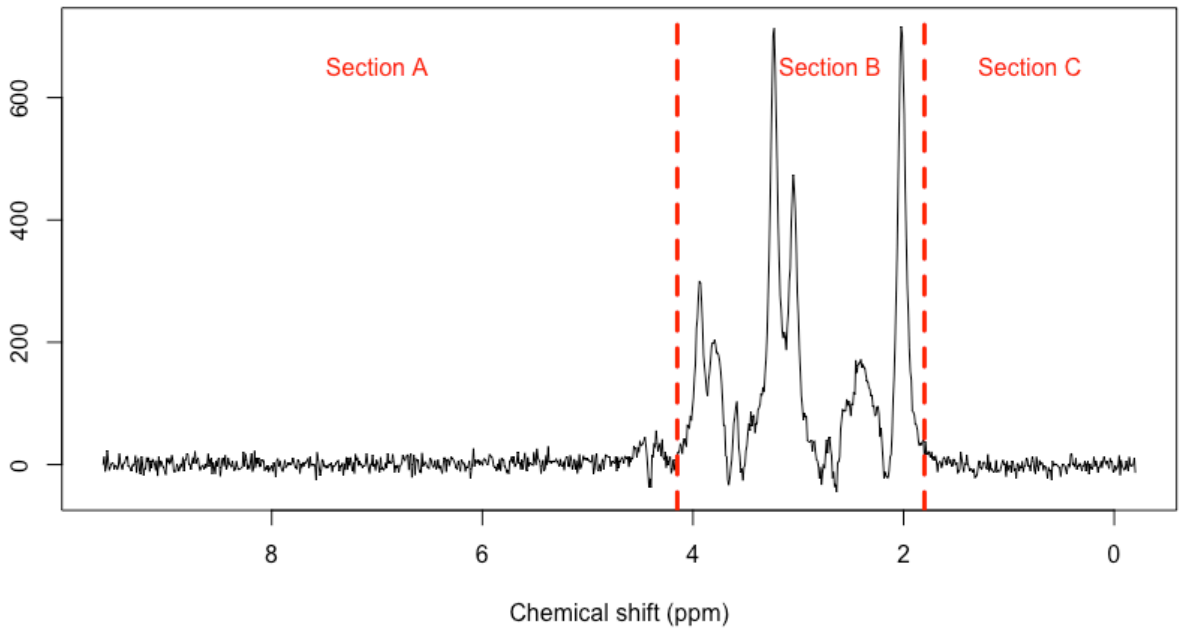

Figure 3.3. Sections of an *in vivo* ^{1}H-MRS spectrum. Sections A and C do not contain metabolite amplitudes, and section B contains metabolite amplitudes.

1. First, a smoothed Spectrum1 for sections A and C, shown in Figure 3.5.A, was obtained by applying a moving mean filter, followed by a cubic spline interpolation. A window size of around 1.5% of the length of the signal was implemented for the filter. For the interpolation, we set a window of nearly 7% of the length of the signal (e.g., 64 points for a signal with 1,024 points). The selected points were equidistant, and the first and last points matched the ones of the input spectrum to avoid interpolation errors.

2. Second, a Spectrum2, shown in Figure 3.5.B, computed from a truncation of the time-domain signal at the 4th zero-crossing. Zero-crossings are preferred over a fixed number of points to avoid adding artefacts to the spectrum because of an abrupt truncation of the signal, as shown in Figure 3.6.A.

3. Spectrum3 and Spectrum4, shown in Figure 3.5.C and 3.5.D, respectively, were obtained from a minimisation algorithm. The estimated signals from spectra 3 and 4 are shown in Figure 3.6.B and 3.6.C, respectively. The objective function is defined from equation (2.1), where the parameters to be found are the frequencies θ_1, θ_2 of the periodic component and the amplitude A (see equation (4.1)). We decided to optimise with two frequencies to reduce overestimation of the

baseline, but this minimisation step could also be studied for three or more frequencies. In equation (4.1), the imaginary components are denoted with i, and t is the time vector.

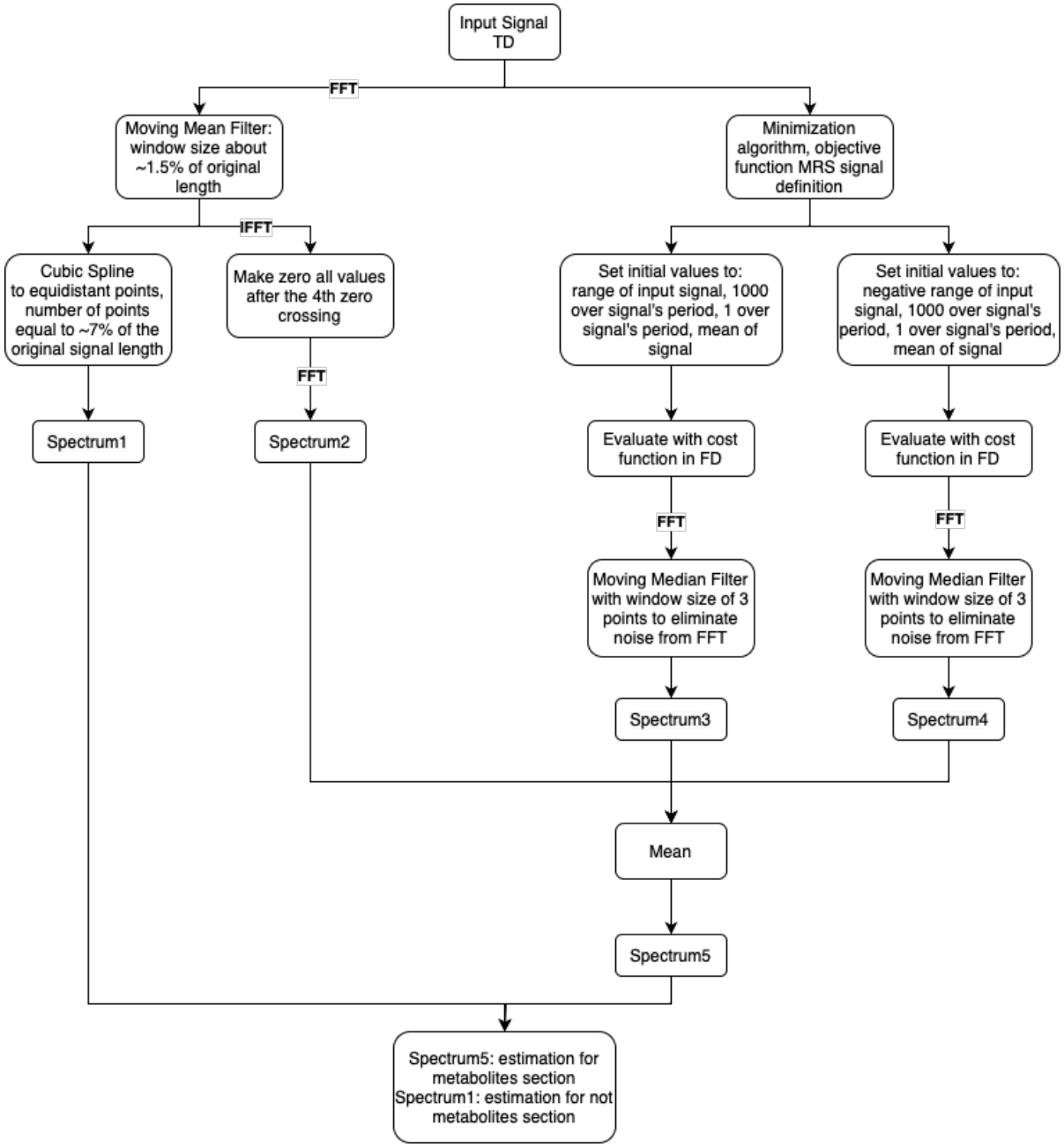

Figure 3.4. Pipeline of the proposed method.

$$f_{periodic}(t) = A(\sin(\theta_1 2\pi t)i + \cos(\theta_1 2\pi t) + \sin(\theta_2 2\pi t)i + \cos(\theta_2 2\pi t)) \qquad (4.1)$$

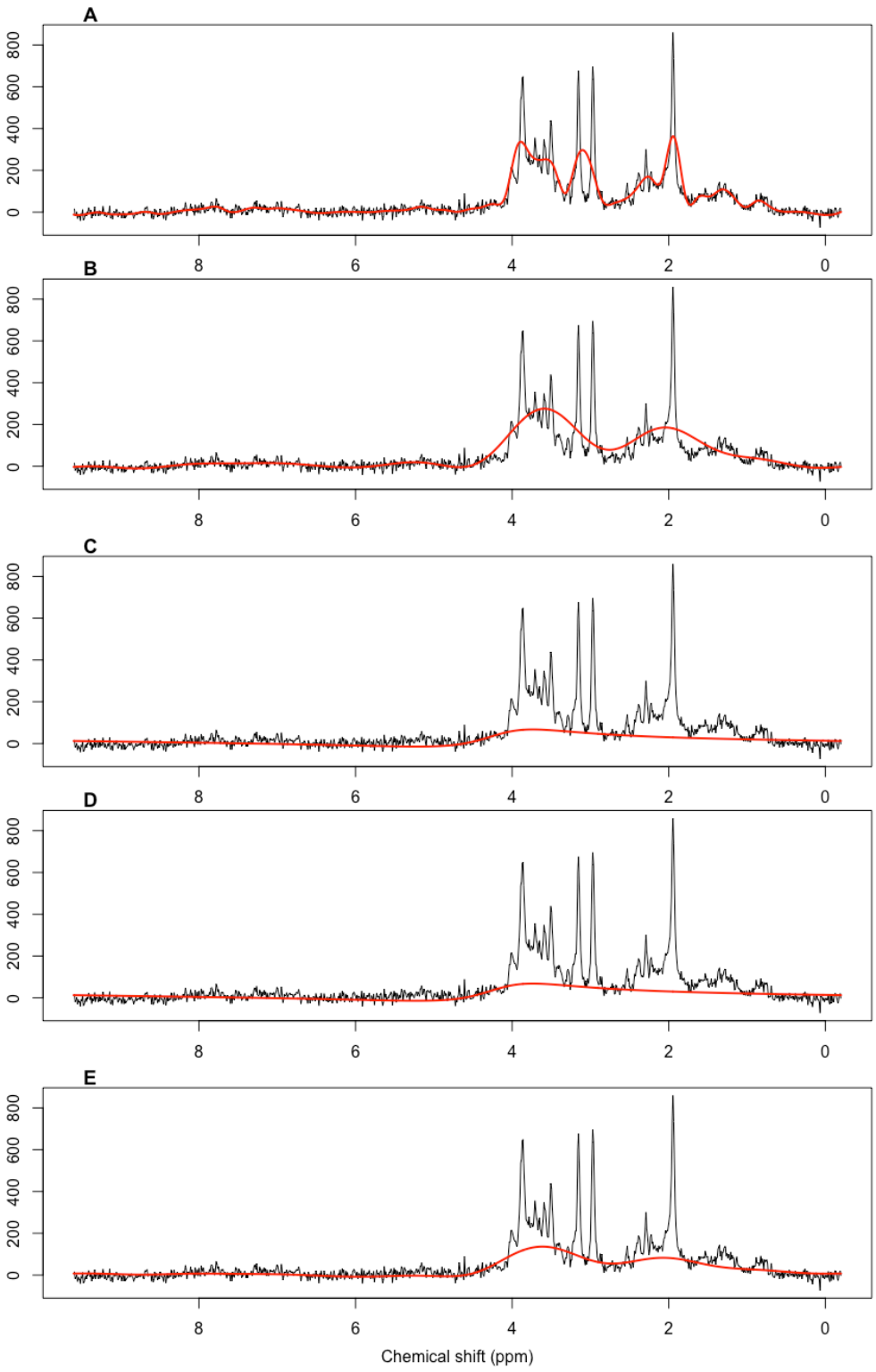

Figure 3.5. Pre-estimated spectra for the proposed method. **A**: Spectrum1, from the moving mean filter in FD. **B**: Spectrum2, from truncation in TD. **C**: Spectrum3, from the minimisation step. **D**: Spectrum4, from the minimisation step. **E**: Spectrum5, mean between Spectra 2, 3, and 4.

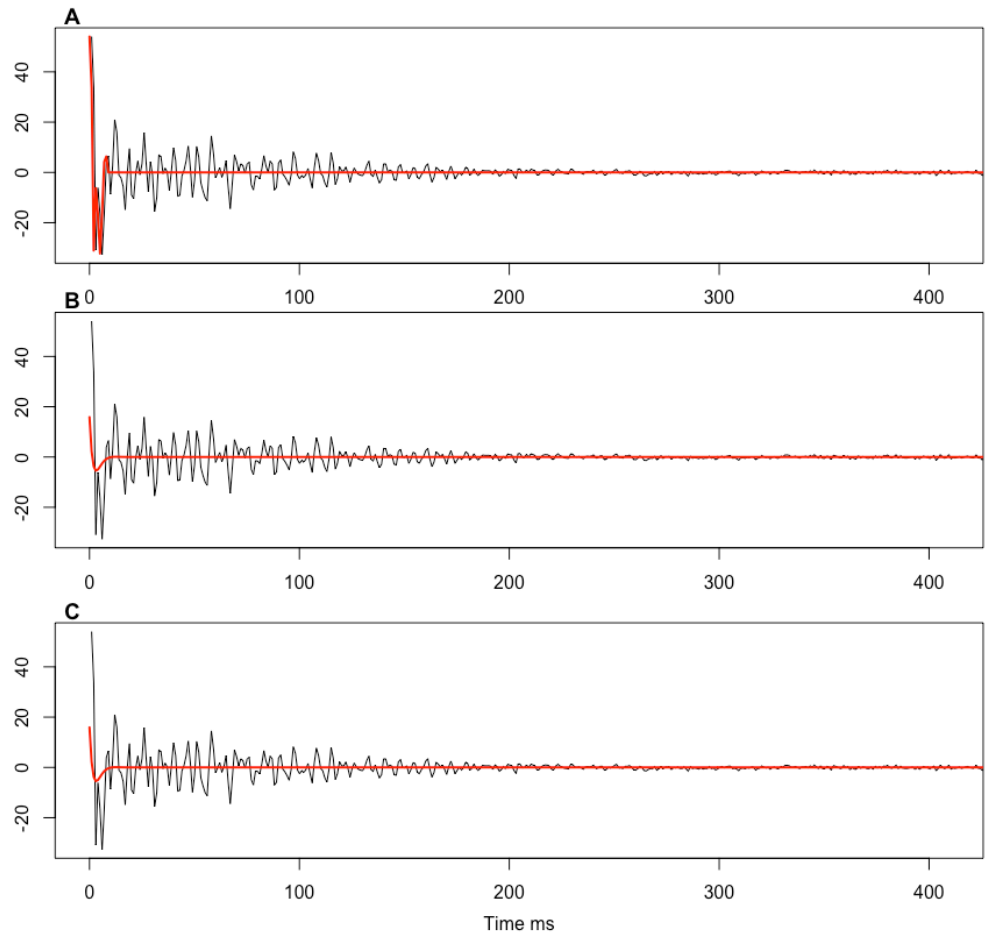

Figure 3.6. Pre-estimated signals for the proposed method. **A**: Signal2, from truncation in TD. **B**: Signal3, from the minimisation step. **C**: Signal4, from the minimisation step.

According to the SOTA, the signal is affected by the baseline in the first points of the FID; therefore the exponential component λ was re-written to force the estimated baseline in TD to be extremely close to zero after the middle point of the signal (see equation (4.2)).

$$f_{exponential}(t) = \exp\left(\frac{\ln\left(10^{-100}\right)}{t_E}t\right) \tag{4.2}$$

Then, λ was calculated by assuming equation (4.2) close to zero after time t_E:

$$\exp(-\lambda t_E) \approx 0 \longrightarrow \exp(-\lambda t_E) = 10^{-100}$$

$$\Longrightarrow -\lambda t_E = \ln(10^{-100})$$

$$\Longrightarrow -\lambda = \frac{\ln(10^{-100})}{t_E}$$

Then, the objective function is obtained from the multiplication of both equations (4.1) and (4.2), plus an offset value:

$$f_{objectiveFunc} = f_{periodic}(t) f_{exponential}(t) + offset \qquad (4.3)$$

The final expression for our objective function involves the amplitude A and the frequencies θ_1, θ_2 as the parameters to be minimised:

$$argmin_{A,\theta_1,\theta_2}\left(A\left(\sin\left(\theta_1 2\pi t\right) i + \cos\left(\theta_1 2\pi t\right) + \sin\left(\theta_2 2\pi t\right) i + \cos\left(\theta_2 2\pi t\right)\right)\exp\left(\frac{\ln\left(10^{-100}\right)}{t_E} t\right) + offset\right)$$

The initial parameters are set automatically according to the input signal:

(a) The amplitude A is the range of the signal (i.e., the difference between maximum and minimum values). A positive range is used for Spectrum3, and a negative range is used for Spectrum4 to consider a baseline with a starting value below zero.

(b) The frequencies θ_1, θ_2 are set as indicated in equations (4.4) and (4.5). The term T corresponds to the average period of the signal. To calculate T, first, we computed the distance between two zero crossings of the signal in TD, we repeated this for every following zero crossing, and finally, we computed the average of those distances to obtain T. We chose to start from two different frequencies (θ_2 100 times higher than θ_1) to address both smiley artefacts (high frequencies) and broad components at the metabolite range (lower frequencies).

$$\theta_1 = \frac{1}{T} \qquad (4.4)$$

$$\theta_2 = \frac{100}{T} \qquad (4.5)$$

(c) The offset is set as the average value of the signal, which will be equal to zero for our data.

The cost function was defined as the norm between the input spectrum $s(k)$ and estimated baseline $f(k)$, both of length N, P_1 as the limit between sections A and B, and P_2 as the limit between sections B and C. Then, the loss L is computed as:

$$L_1(s,f) = \sum_{k=0}^{P_1}\left(s(k) - f(k)\right)^2 + \frac{1}{\sum_{k=P_1+1}^{P_2}\left(s(k) - f(k)\right)^2} + \sum_{k=P_2+1}^{N}\left(s(k) - f(k)\right)^2$$

$$L_2(s,f) = \sum_{k=0}^{N}\left(|s(k)| - |f(k)|\right)^2$$

$$L(s,f) = \left(L_1(s,f) + L_2(s,f)\right) \tag{4.6}$$

4. Finally, the smoothed spectrum was used in sections A and C, and the mean between the spectrum2, spectrum3, and spectrum4, shown as spectrum5 in Figure 3.5.E, was used in section B. The union of these three sections is performed using two vectors: (1) *ones* for sections A and C, *zeros* for section B, and (2) *zeros* for sections A and C, *ones* for section B. For a smooth transition at the limits of each section, the vectors gradually change from *one* to *zero* (and from *zero* to *one*) in a range of 50 points. To determine the points (P_1, P_2) that separate each section, a moving standard deviation window is used to determine a threshold to discard the metabolite amplitudes, following the diagram in Figure 3.7.

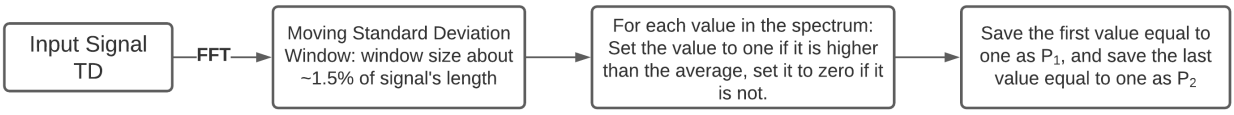

Figure 3.7. Pipeline for determining the limits of each section of the spectrum.

3.3. RMSE on simulation with the designed algorithm

The designed algorithm was tested with the simulated signals presented previously and compared against the four SOTA algorithms. The new results from estimating the simulated baselines are shown in Figure 3.8.

The proposed method did perform slightly better than airPLS and ABfit but still retrieved higher RMSE than CWT and BRCI. Our proposed method had an average RMSE of 96.56 for the whole

signal. When comparing the average RMSE in the metabolites section, the best result was achieved by CWT with 66.67, followed by our method with 94.23, then BRCI with 95.91, airPLS with 171.81, and the highest being ABfit with 213.78.

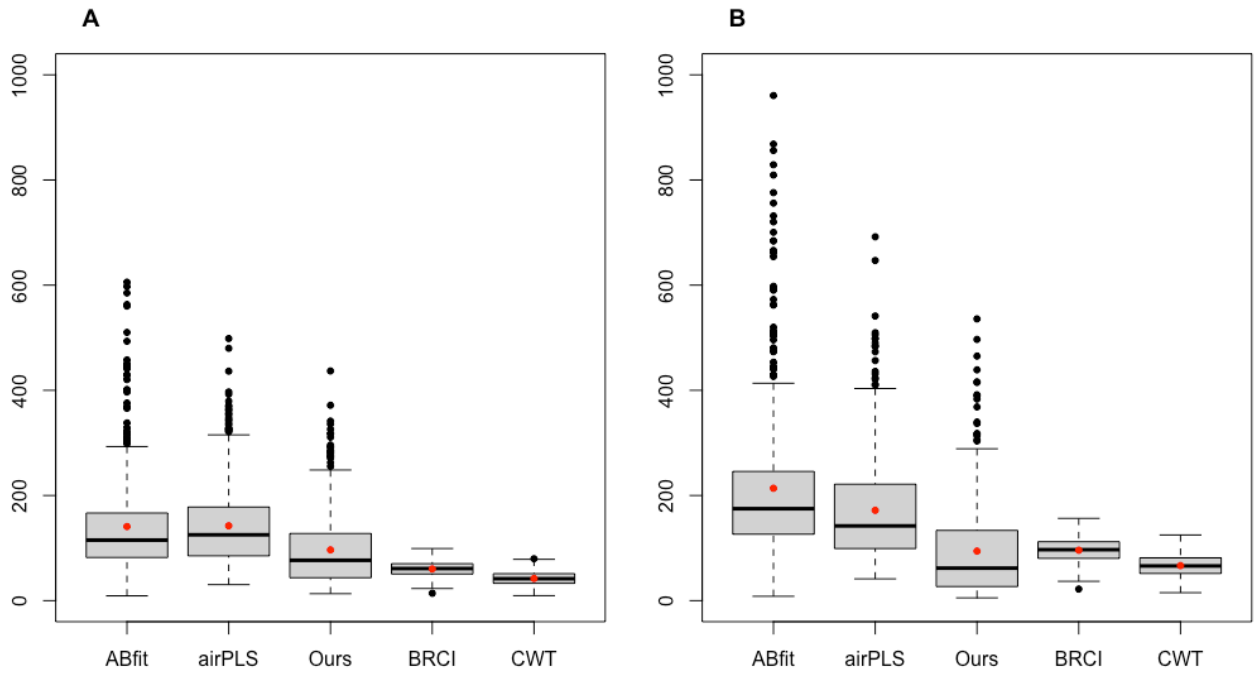

Figure 3.8. RMSE between simulated and estimated baselines using ABfit, airPLS, BRCI, CWT, and **our proposed algorithm**. **A**: RMSE from the 1,024 values of each signal. **B**: RMSE from 400 values in the metabolite section from 4.7048 ppm to 0.8825 ppm of each signal. The mean RMSE of the 500 estimated baselines is plotted as a red point.

4. Chapter 4. Algorithm evaluation

4.1. Evaluation setup

To compare the SOTA algorithms to our proposed algorithm, the five steps presented in Figure 4.1 were followed: (1) the collection of real datasets, (2) the pre-processing of the signals with the same water suppression algorithm, (3) the application of the baseline correction algorithm, (4) the estimation of the fits with the same spectral fitting model, (5) computation of the FQN for each signal in each dataset. In this setup, all signals were processed with the same algorithms and models, except the five baseline correction algorithms, allowing us to compare the FQN to determine which algorithm has the best impact for fitting the amplitudes of the molecules.

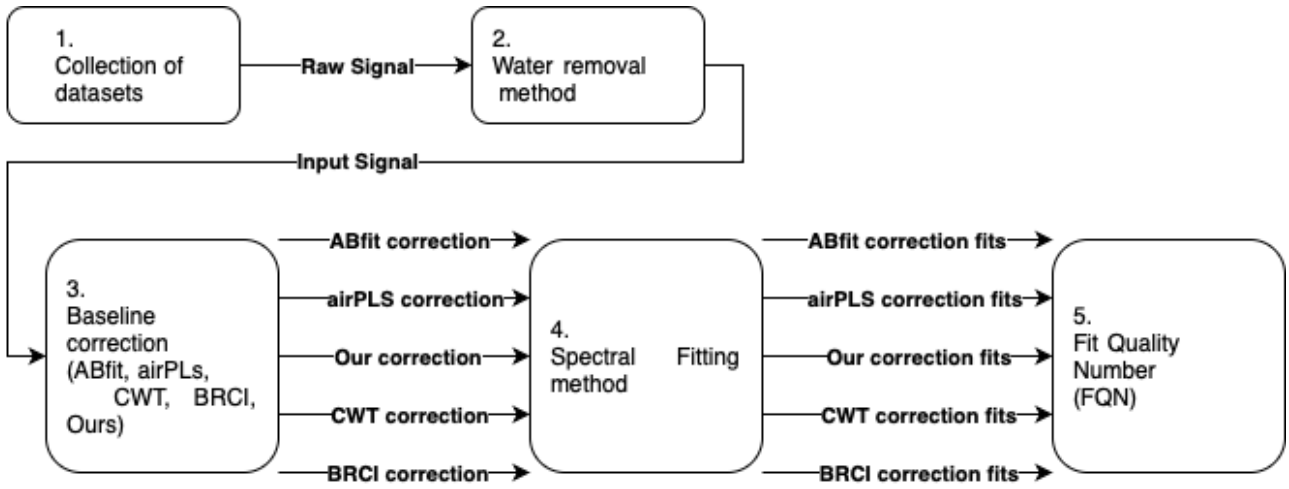

Figure 4.1. Evaluation setup for algorithms comparison.

4.2. Real data characterisation

Datasets from fourteen subjects were used for the testing of the algorithms, from which thirteen were semiLASER MRSI datasets at 3T with 40ms TE, and one was PRESS MRSI datasets at 1.5T with 40ms TE; eight corresponded to female subjects and six to male subjects. Ten datasets had 112 signals (or voxels), two had 192 signals, the rest had 256 signals, and all were composed of 1,024 complex values. The data used in this evaluation was anonymised to protect patient privacy. Table 4.1 contains more information of interest on the data used to evaluate the algorithms, such as the diagnosis for each subject.

We used the integrated tools of the SpectrIm-QMRS software package to quantify the datasets. We manually built a spectral model (i.e., ideal spectral representation of the metabolite amplitudes in a dataset) for datasets Generic1 to Generic10, and another spectral model for datasets Generic11, Generic 12, and Generic13. We could not implement a spectral model for dataset Generic14, because it required a higher knowledge and longer construction time. We only performed a visual analysis of the results for dataset Generic14. The spectral models comprised 13 metabolites components (including NAA-CH_3, Cr-CH_3, CH_3, etc.). The spectral models were applied once to the baseline-corrected data for each dataset, using each baseline correction method. We also quantified the data without correction for datasets Generic1 to Generic10.

Table 4.1. Description list of real data used for comparison part 2.

Subject	Sex	Age (Years)	Diagnosis	IDH	LOH	MGMT	Sequence	B-field	TE	N° Signals
Generic1	M	61	H.C.	N.A.	N.A.	N.A.	semiLASER	3T	40 ms	112
Generic2	M	48	H.C.	N.A.	N.A.	N.A.	semiLASER	3T	40 ms	112
Generic3	F	57	H.C.	N.A.	N.A.	N.A.	semiLASER	3T	40 ms	112
Generic4	F	60	H.C.	N.A.	N.A.	N.A.	semiLASER	3T	40 ms	112
Generic5	F	63	H.C.	N.A.	N.A.	N.A.	semiLASER	3T	40 ms	112
Generic6	M	63	H.C.	N.A.	N.A.	N.A.	semiLASER	3T	40 ms	112
Generic7	F	50	H.C.	N.A.	N.A.	N.A.	semiLASER	3T	40 ms	112
Generic8	M	67	H.C.	N.A.	N.A.	N.A.	semiLASER	3T	40 ms	112
Generic9	M	59	H.C.	N.A.	N.A.	N.A.	semiLASER	3T	40 ms	112
Generic10	F	68	H.C.	N.A.	N.A.	N.A.	semiLASER	3T	40 ms	112
Generic11	M	64	H.C.	N.A.	N.A.	N.A.	semiLASER	3T	40 ms	192
Generic12	F	68	AC-g2	+	N.A.	N.A.	semiLASER	3T	40 ms	256
Generic13	F	53	MS	N.A.	N.A.	N.A.	PRESS	1.5T	30 ms	256
Generic14	F	71	GBM	-	+	-	semiLASER	3T	40 ms	192

Abbreviations: Female (F), Male (M), positive diagnosis (+), negative diagnosis (-), Not applicable (N.A.), Glioblastoma Multiforme (GBM), Anaplastic Oligodendroglioma (AO), Astrocytoma Grade II (AC-g2), Multiple Sclerosis (MS), Healthy Control (H.C.), Intradialytic hypotension (IDH), Loss of heterozygosity (LOH), protein O(6)-Methylguanine-DNA-methyltransferase (MGMT), milliseconds (ms).

4.3. Results

Estimated baselines with our method for the absorption channel of signals in datasets Generic12 and Generic14 are presented in Figures 4.2 and 4.3, respectively, including the results for the algorithms ABfit, airPLS, CWT, and BRCI for comparison. Figure 4.4 presents the baseline estimation for the dispersion channel of a signal in dataset Generic12., Figure 4.5 shows the Magnitude and Phase of the corrected spectrum of a signal in dataset Generic12.

In Figure 4.6, we show the FQN map over the CSI data for the NAA-CH_3 component in dataset Generic1. The voxels represent the signals in dataset Generic1. The colour in each voxel varies per algorithm. The colour range was scaled from the minimum to the maximum FQN obtained by the algorithm presented in a map. Therefore, each colour range is different in each colour map. The FQN obtained for a single voxel is represented by a two-decimal number over the voxel.

The box plot in Figure 4.7 summarizes the FQNs results obtained by each tested algorithm for datasets Generic1 to Generic10. We included the FQN result when no correction was applied prior to quantification.

The box plot in Figure 4.8 contains the execution time per signal of the evaluation for each algorithm. On average, the lowest execution time per signal was achieved by airPLS with 5.95ms, followed closely by BRCI with 9.56ms, then CWT with 85.60ms, and our method with 223.85ms, the slower being ABfit with 31.870s.

In the case of datasets Generic11, Generic12, and Generic13, the output of the quantification tool did not return the FQNs for each voxel. Table 4.2 contains the minimum and maximum FQN, the mean, standard deviation, skewness, and kurtosis, for datasets Generic11, Generic12, and Generic13.

Finally, Table 4.3 contains the average loss (L) of Spectrum3 (L_3) and Spectrum4 (L_4) from our proposed method for each dataset.

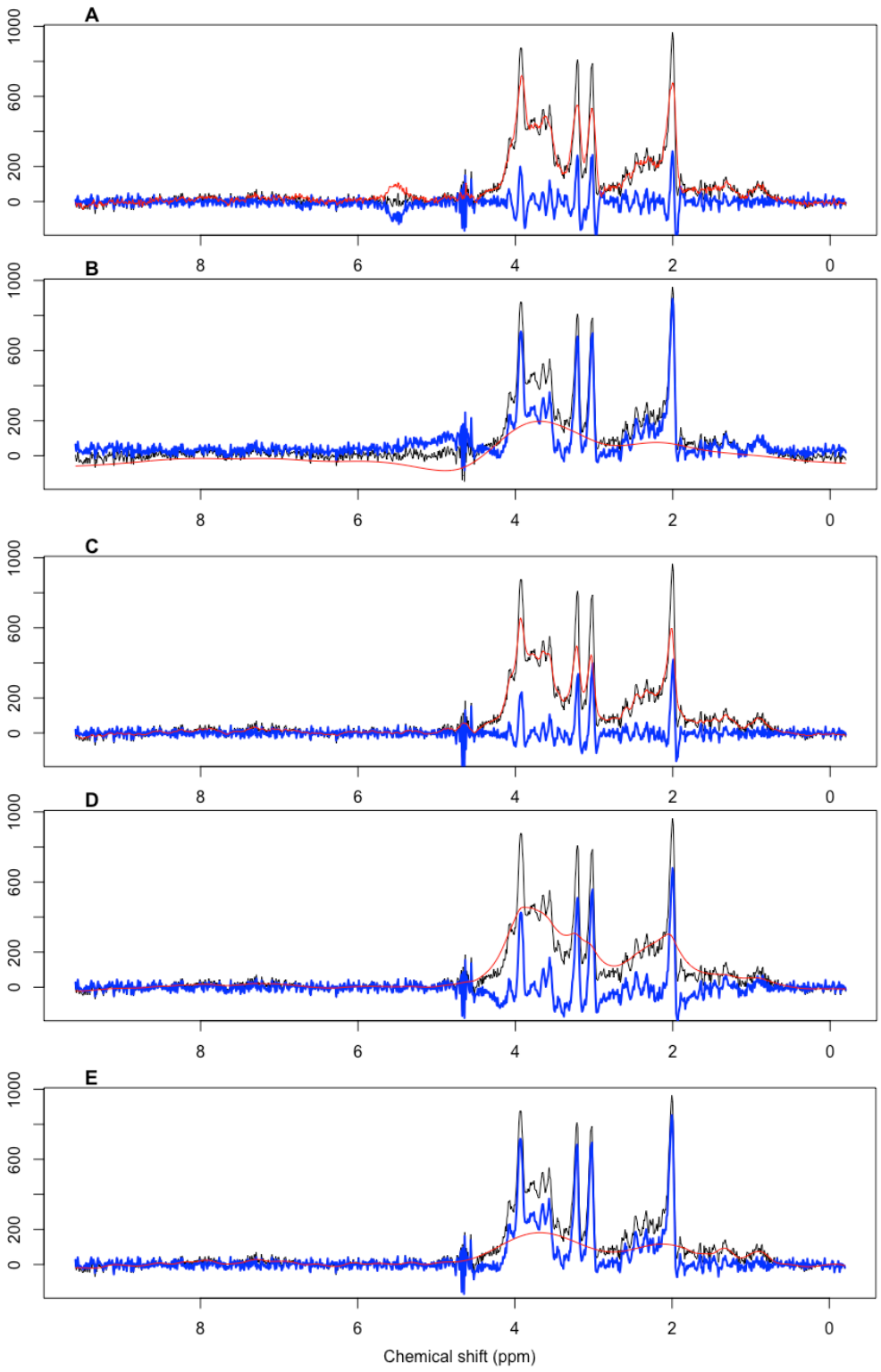

Figure 4.2. Baseline estimations (red) and spectrum corrections (blue) for absorption channel of input spectrum n°1 (black) in dataset Generic12. Estimates made with (**A**) ABfit, (**B**) airPLS, (**C**) CWT, (**D**) BRCI, and (**E**) our method.

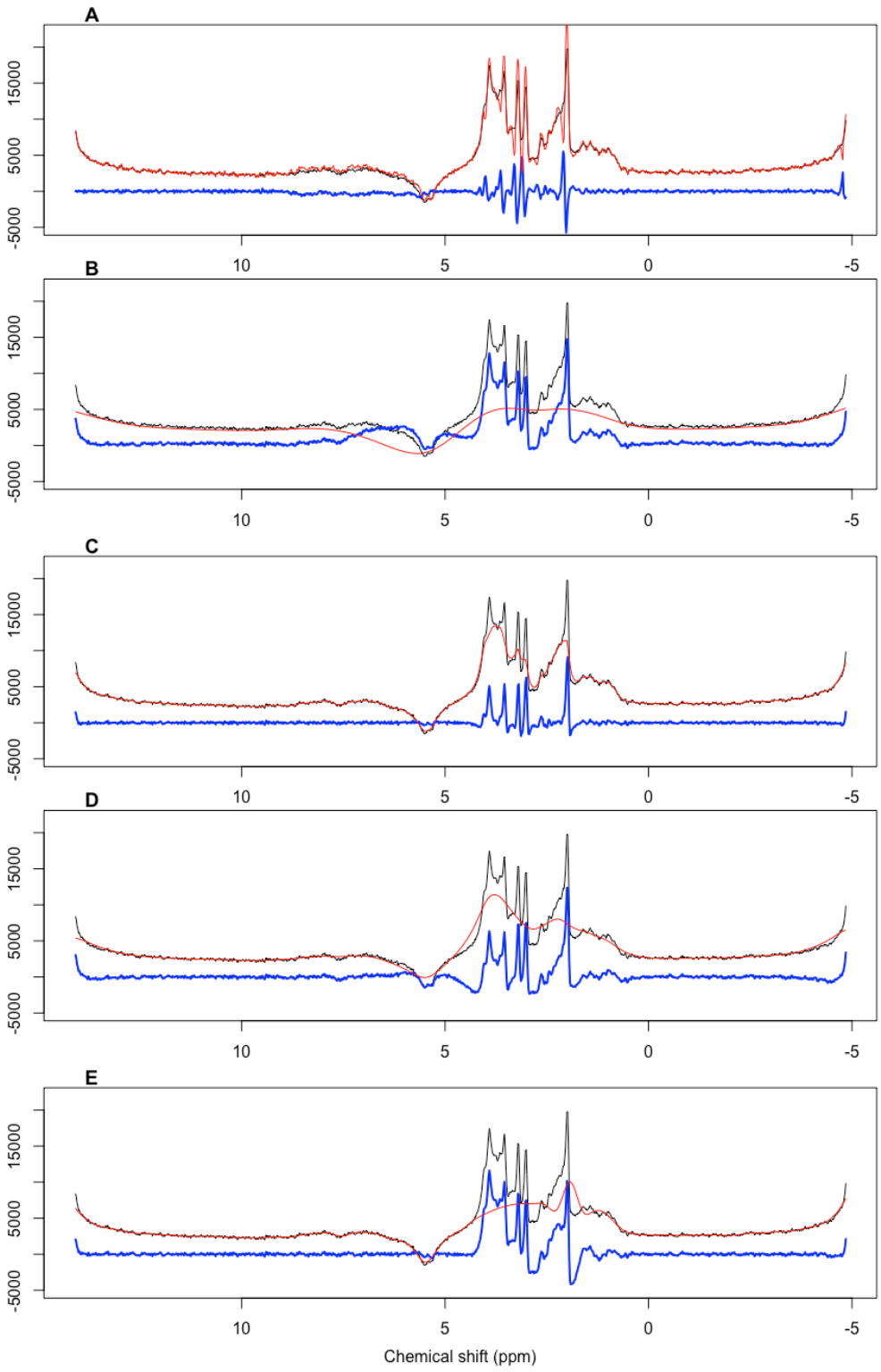

Figure 4.3. Baseline estimation (red) and spectrum corrections (blue) for absorption channel of input spectrum n°1 (black) in dataset Generic14. Estimations made with (**A**) ABfit, (**B**) airPLS, (**C**) CWT, (**D**) BRCI, and (**E**) our method.

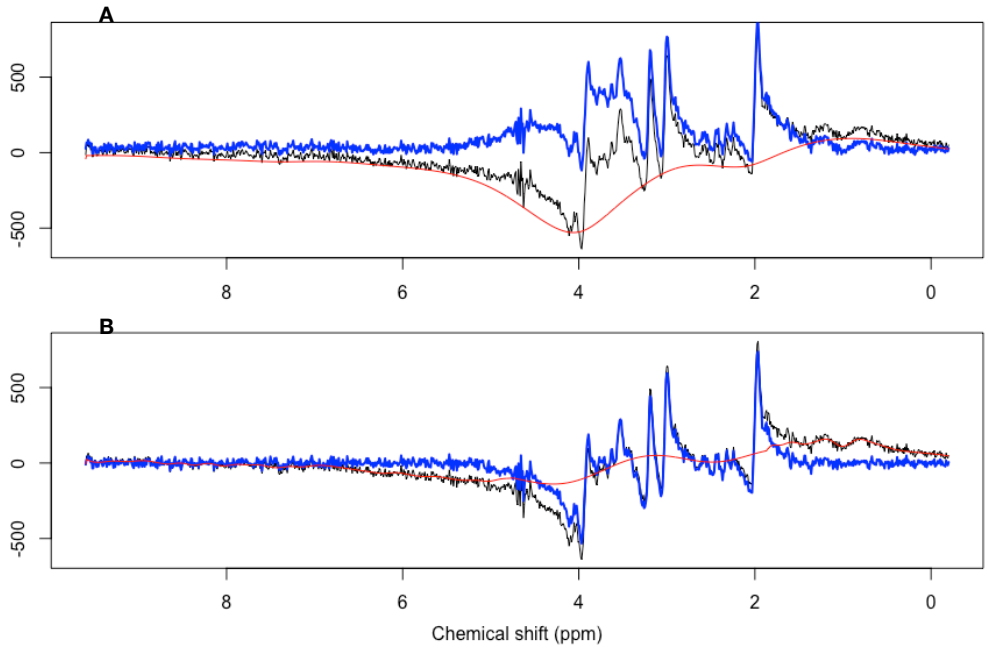

Figure 4.4. Baseline estimation (red) and spectrum corrections (blue) for dispersion channel of input spectrum n°1 (black) in dataset Generic12. Estimations made with (**A**) ABfit, (**B**) airPLS, (**C**) CWT, (**D**) BRCI, and (**E**) our method.

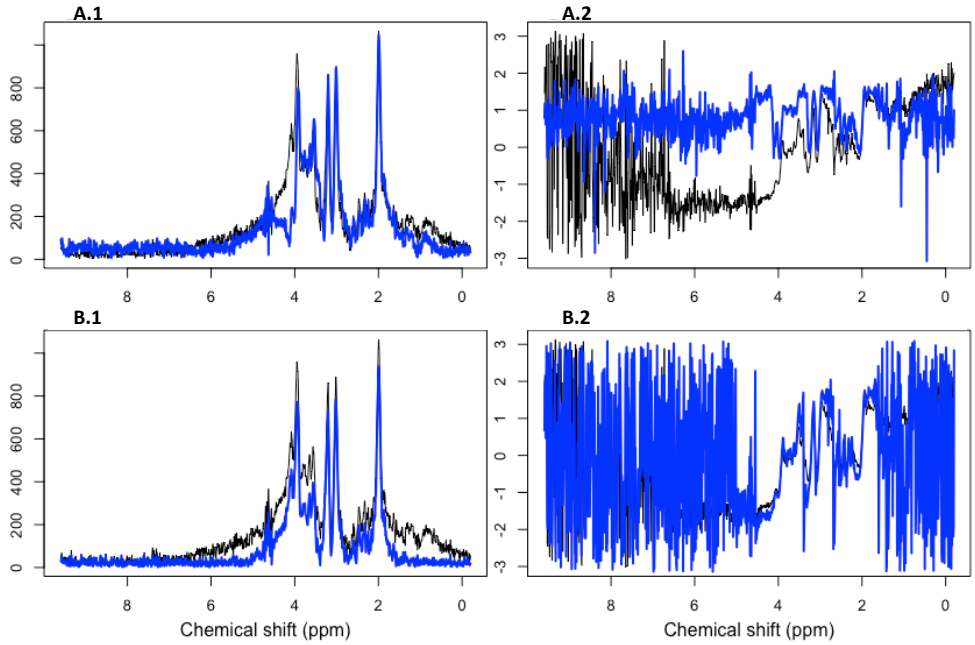

Figure 4.5. Magnitude (Left) and Phase (Right) of the corrected spectrum (blue) for input spectrum n°1 (black) in dataset Generic12. Corrections were made with (**A**) ABfit, (**B**) airPLS, (**C**) CWT, (**D**) BRCI, and (**E**) our method.

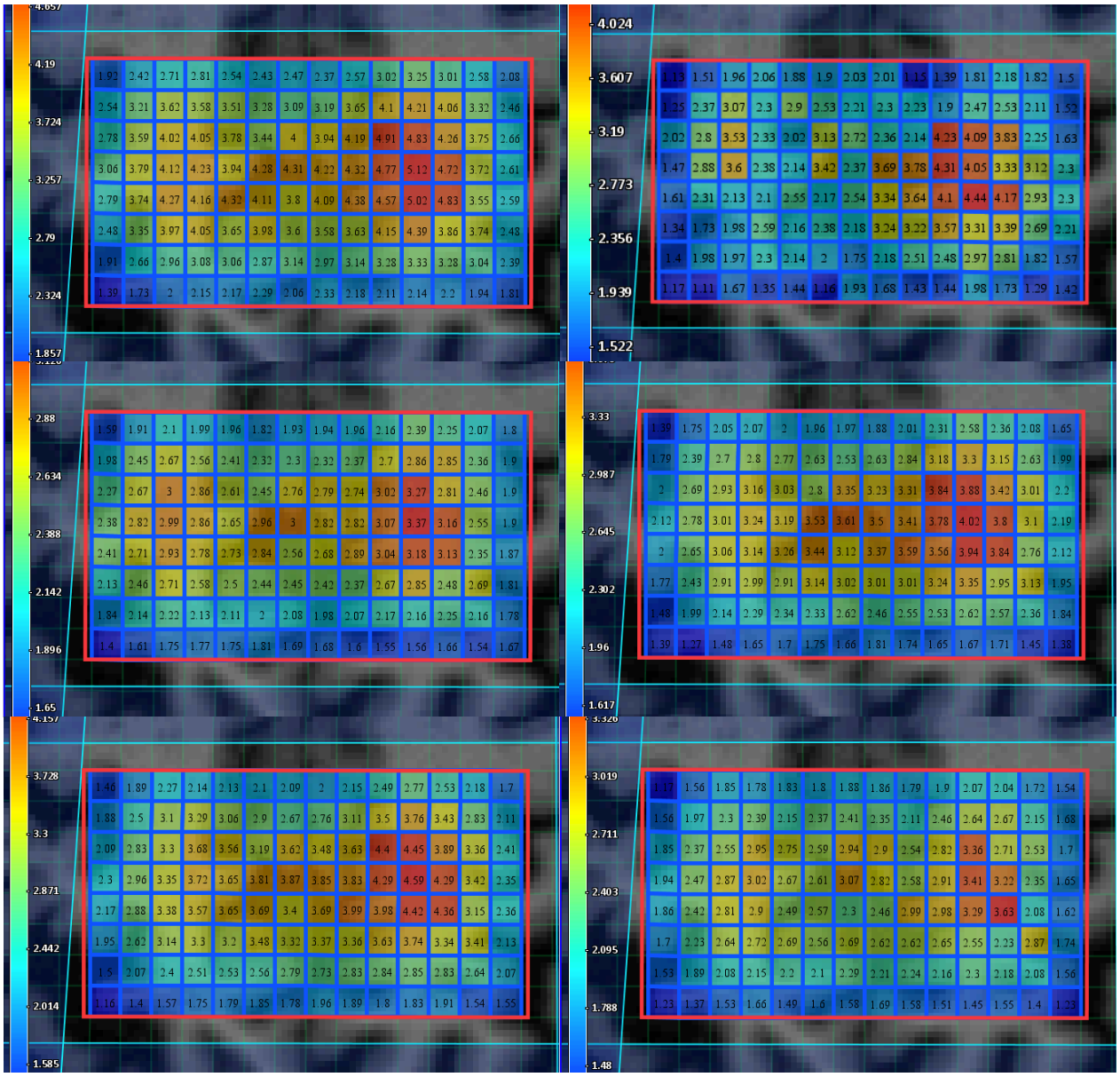

Figure 4.6. FQN map displayed over CSI data (NAA-CH_3 component) computed before baseline correction (Top-Left), and after correction with ABfit (Top-Right), airPLS (Middle-Left), BRCI (Middle-Right), CWT (Bottom-Left), and our method (Bottom-Right). Each colour map has a different range; the strongest red box in a map corresponds to the highest FQN obtained by that correction method, and the same for the strongest blue box.

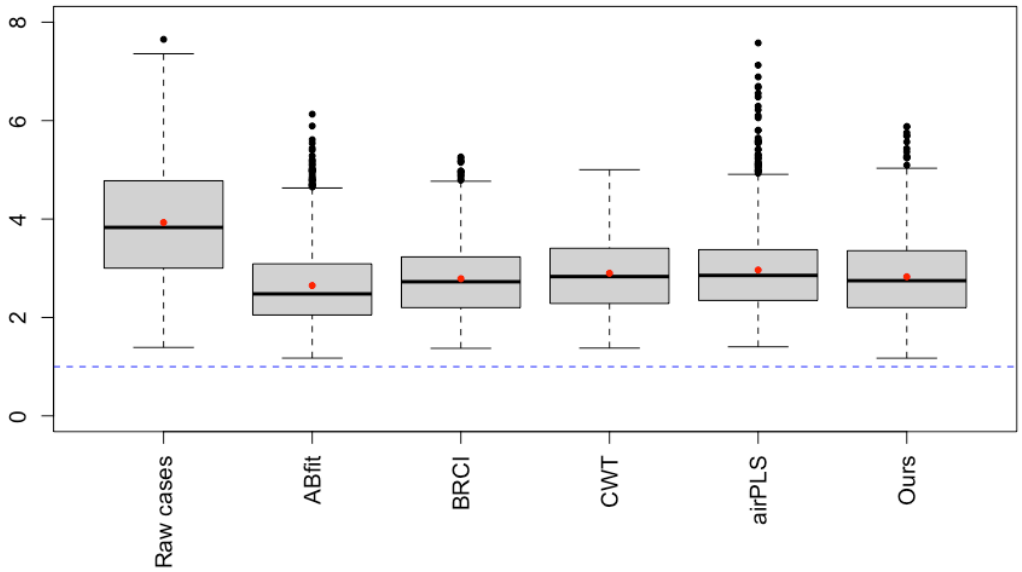

Figure 4.7. FQN results for datasets Generic1 to Generic10.

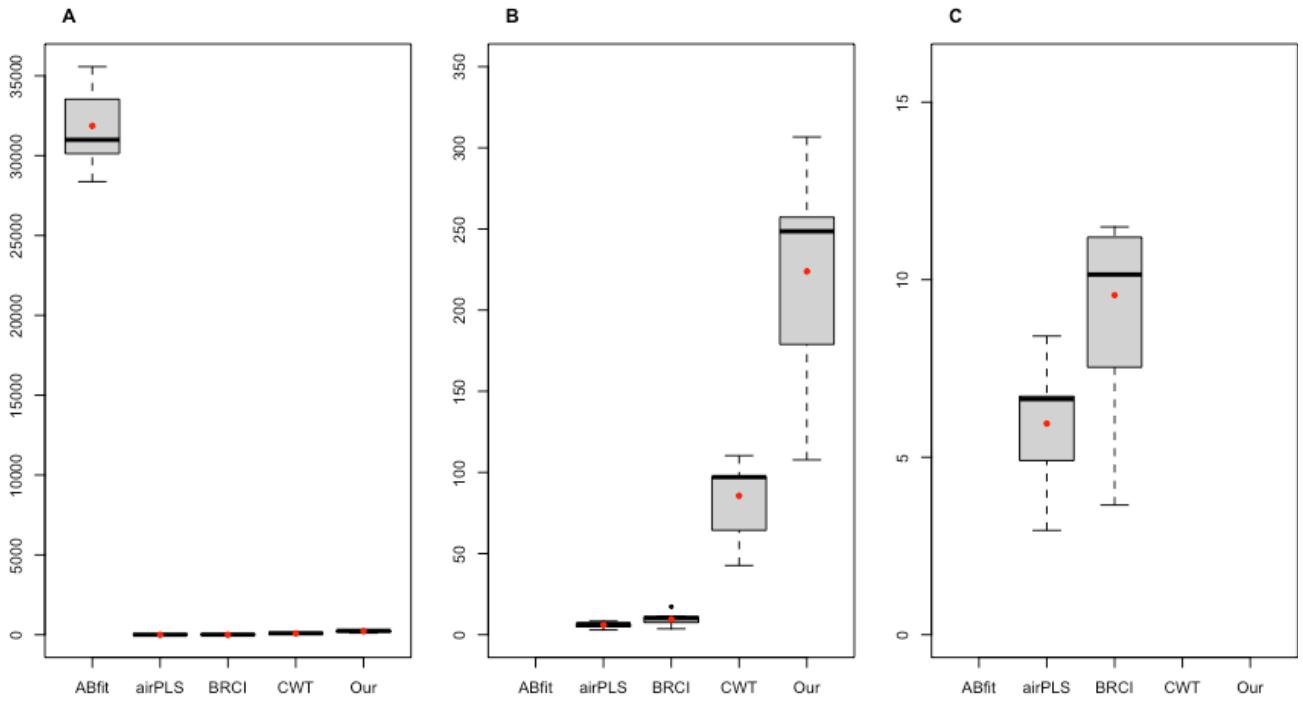

Figure 4.8. Execution time in milliseconds (ms) of the implemented methods (ABfit, airPLS, BRCI, CWT, and Ours) for every signal corrected in all 14 datasets. Box plots are scaled in different ranges to show the different execution time boxes. A: scaled from 0ms to 36000ms. B: scaled from 0ms to 350ms. C: scaled from 0ms to 16ms.

Table 4.2. FQN results of evaluating proposed method and state-of-the-art methods

	Method	Min	Max	Mean	Std Dev
Generic11	airPLS	1.39	4.31	3.25	0.68
	CWT	**1.14**	4.00	2.81	0.70
	Ours	1.22	**2.71**	**2.01**	0.32
Generic12	airPLS	0.90	4.70	2.35	0.73
	CWT	**1.07**	5.01	2.10	0.60
	Ours	0.59	**4.15**	**1.73**	0.67
Generic13	airPLS	**0.90**	4.70	2.35	0.73
	CWT	1.13	**2.63**	**1.78**	0.33
	Ours	1.20	3.27	1.88	0.34

Observation: The results correspond to the FQNs obtained for the complete dataset.

Table 4.3. The average loss L of Spectra 3 and 4 from our proposed method.

	L_3	L_4
Generic1	$3.96 \cdot 10^6$	$4.20 \cdot 10^6$
Generic2	$3.95 \cdot 10^6$	$4.03 \cdot 10^6$
Generic3	$3.90 \cdot 10^6$	$3.91 \cdot 10^6$
Generic4	$2.81 \cdot 10^6$	$2.28 \cdot 10^6$
Generic5	$2.45 \cdot 10^6$	$2.48 \cdot 10^6$
Generic6	$5.61 \cdot 10^6$	$5.75 \cdot 10^6$
Generic7	$4.02 \cdot 10^6$	$4.06 \cdot 10^6$
Generic8	$2.93 \cdot 10^6$	$2.91 \cdot 10^6$
Generic9	$3.91 \cdot 10^6$	$4.14 \cdot 10^6$
Generic10	$4.53 \cdot 10^6$	$4.53 \cdot 10^6$
Generic11	$5.87 \cdot 10^6$	$5.87 \cdot 10^6$
Generic12	$5.42 \cdot 10^6$	$5.48 \cdot 10^6$
Generic13	$6.95 \cdot 10^6$	$6.68 \cdot 10^6$

Generic14	$2.48 \cdot 10^9$	$2.76 \cdot 10^9$

Observations: Spectrum3 loss (L_3), Spectrum4 loss (L_4).

4.4. Discussion

The estimated baselines presented in Figures 4.2 and 4.3 show that the proposed method not only performs as well as the SOTA algorithms at section B with metabolite amplitudes but also does not have a negative impact on the other section where the baseline is much easier to estimate. Moreover, airPLS and CWT are susceptible to remaining water amplitudes, or the lactate peak that commonly appears with short TE, as shown in Figure 4.2.

As observed in Figure 4.3, our proposed method also has good flexibility on different spectrum shapes, depending on the pulse sequence and TE chosen to acquire the signals. Compared to airPLS, using a moving mean filter does not negatively impact sections A and C, where the baseline can be easily estimated with a moving mean filter.

The proposed method also performs well for estimating the baseline at the dispersion spectrum, as shown in Figure 4.4. When analysing the Magnitude and Phase of the corrected spectra shown in Figure 4.5, we can observe that all SOTA algorithms do change the phase at the metabolites section of the spectrum. In contrast, our method positively changes the phase at sections A and C but maintains mostly similar the phase at sections. This is a good indication of the low negative impact our method has on the original signal.

Something that must be studied and improved is the L value, reported in Table 4.3, from the minimisation step, which is too high. Although, this is expectable given the cost function from equation (4.6). If L is equal to zero, then the output result from the minimisation would be equal to the input signal. However, we are looking for an estimation of the baseline, matching most of the input signal by using only two frequencies. Therefore, in this case, L will never be equal to the input signal, and probably be a high value.

The FQN results generally show that the proposed method performs better than the SOTA algorithms. When analysing the values reported in Table 4.2, the proposed method returned FQNs more uniform and closer to 1 than airPLs and CWT. This means that combining the smoothing filter

with time-domain information improves the correction. Also, when looking at the colour map of Figure 4.6, the FQNs obtained with our method are more uniform than the ones obtained with the other two SOTA algorithms. This conclusion is evident in Figure 4.7, where our approach obtained, on average, better performance than airPLS, which is the only other algorithm that estimates the baseline for the complex values of the signal. Even when ABfit, BRCI, and CWT obtained better FQN results, these algorithms only estimated the baseline for the absorption channel. Therefore, these algorithms are instantly discarded.

Another advantage of the algorithm is the good performance it can achieve when used with its pre-defined parameters. In contrast, half of the SOTA algorithms require more predefined setups (which were all suggested by their authors). ABfit requires a spectral model as input, which makes it the most complicated of the four SOTA algorithms. Alternatively, the author provides a function for a basis spectral model depending on the MRS data type, which can help to speed up the input process, but is not yet the ideal. For instance, airPLS requires five parameters: a smoothing parameter, the order of the difference of penalties, a weight exception proportion value, an asymmetry parameter, and the maximum iterations. The user must adjust these parameters depending on the MRS input dataset and, in some cases, for each signal. CWT and BRCI require fewer and easy-to-implement parameters. CWT can be used fully automatically, but the user can also modify the threshold scale factor, which is used to determine different peaks that will impact the final baseline estimation. BRCI can also be used fully automatically, but the user can change flags to include broad peak detection if needed.

5. Chapter 5: Conclusions

5.1. Summary

This thesis presents a new method for baseline correction algorithm for quantification of *in vivo* ^{1}H-MRS. The proposed method performs the baseline estimation by combining time-domain and frequency-domain approaches. These approaches were applied depending on the section of the spectrum. A moving mean filter was applied to sections A and C (without metabolite amplitudes), which, according to the literature research, is still one of the simplest yet effective approaches for estimating the baseline in the mentioned sections. For section B (with metabolites), a combination of three baselines is used: one estimated by truncation of the signal in TD and the other two obtained with a minimisation function. The complete description of the method is shown in Figure 3.4.

Twenty algorithms were found in the literature review, presented in Tables 2.1 and 2.2, from which only four were found to meet the requirements presented in the Methodology of this thesis: ABfit, airPLS, BRCI, and CWT. They were implemented in MATLAB and RStudio to compare their performance against our proposed method.

The evaluation consisted in comparing the performance of the algorithms with real data. We collected fourteen datasets described in Table 4.1. The setup consisted of pre-processing and quantifying the data with the same methods, being the baseline correction the only step with different methods applied to the datasets. The Fit Quality Number (FQN) was set as a comparison metric. Overall, the best results were achieved by our method when directly compared to airPLS, which is the only SOTA method that also performs baseline correction for complex values of the signal.

5.2. Conclusion

At the end of this thesis, the main objective of this thesis and the three specific objectives were accomplished. We built an algorithm for baseline correction of brain ^{1}H-MRS spectra by including analysis in Time and Frequency Domain. To do so, we identified the most common and important artefacts in ^{1}H-MRS brain signals, e.g. ‘smiley-artefacts’, among others shown in Figure 2.4, and the

available methods for baseline correction for ^{1}H-MRS spectra, presented in Tables 2.1 and 2.2. Then we designed and implemented a baseline correction algorithm aiming at improving the complex spectrum without overfitting the estimated baseline, which was proven by the FQN obtained from the evaluation. Lastly, we reported an extensive evaluation of the algorithm with simulated and real data and compared it with state-of-the-art methods.

The main challenge faced in this work was the lack of ground truth data. As mentioned in the literature review, baseline signals can be composed of artefacts from many sources and with unknown features. Therefore, there is no unique estimation, but the main objective is to find an estimation allowing clinicians to obtain the best quantification for their data. This is why we had to consider an evaluation setup to compare our proposed method against the SOTA algorithms without knowing the 'real' baseline, but only the best fit for our data.

Another challenge was related to the few SOTA algorithms found in the literature review that we could use for comparison. Most baseline estimation algorithms were designed to function with a background signal correction or a quantification method. Of the four SOTA algorithms available for comparison, three only perform the baseline estimation in the absorption spectrum, which is a crucial disadvantage compared to our method. The only SOTA algorithm that could be compared with our method was airPLS, which achieved good results in almost no time. But, airPLS requires too many entry parameters, which makes it practically impossible to implement if an automatic process is needed.

Finally, the baseline correction in brain ^{1}H-MRS spectra can be improved in comparison to the performance of the SOTA algorithms by combining TD and FD math approaches. The combination of truncation of the signal, smoothing filters of the spectra, and minimisation function adds more flexibility to the baseline estimation, allowing the user to use the algorithm fully automatically. Also, the proposed algorithm estimates the baseline for the complex values of the signal, being only comparable to one of the tested SOTA algorithms —which slightly outperforms. This feature is a mandatory condition to perform the spectral fitting and quantification of the spectrum for different ^{1}H-MRS spectra.

5.3. Future work

Further work will be focused on improving the performance of the proposed algorithm. The minimisation function can still be improved, focusing on reducing the loss L. Also, a possibility could be an error value to minimise obtained from the magnitude and phase of the spectrum. A robust method to determine the points for the limits of Sections A, B, and C to get a better baseline estimation for edges (more external values to the left and right) of the spectrum. Finally, another goal could be a lower processing time closer to airPLS.

Bibliography

[1] P. B. Barker, A. Bizzi, N. De Stefano, R. Gullapalli, and D. D. M. Lin, "Introduction to MR spectroscopy in vivo," in *Clinical MR Spectroscopy*, 2009, ch. 1, pp. 1-18.

[2] E. B. Cady *et al.*, "NON-INVASIVE INVESTIGATION OF CEREBRAL METABOLISM IN NEWBORN INFANTS BY PHOSPHORUS NUCLEAR MAGNETIC RESONANCE SPECTROSCOPY," *The Lancet,* vol. 321, no. 8333, pp. 1059-1062, 1983, doi: 10.1016/S0140-6736(83)91906-2.

[3] D. Belkic and K. Belkic, *Signal Processing in Magnetic Resonance Spectroscopy with Biomedical Applications*, 1st ed. CRC Press, 2010.

[4] A. Heerschap *et al.*, "In vivo proton MR spectroscopy reveals altered metabolite content in malignant prostate tissue," (in eng), *Anticancer Res,* vol. 17, no. 3a, pp. 1455-60, May-Jun 1997.

[5] P. J. Bolan, M. T. Nelson, D. Yee, and M. Garwood, "Imaging in breast cancer: Magnetic resonance spectroscopy," (in eng), *Breast Cancer Res,* vol. 7, no. 4, pp. 149-52, 2005, doi: 10.1186/bcr1202.

[6] D. Bertholdo, A. Watcharakorn, and M. Castillo, "Brain Proton Magnetic Resonance Spectroscopy: Introduction and Overview," *Neuroimaging Clinics of North America,* vol. 23, no. 3, pp. 359-380, 2013/08/01/ 2013, doi: https://doi.org/10.1016/j.nic.2012.10.002.

[7] P. B. Barker, A. Bizzi, N. De Stefano, R. Gullapalli, and D. D. M. Lin, "Spectral analysis methods, quantitation, and common artifacts," in *Clinical MR Spectroscopy*, 2009, ch. 3, pp. 34-50.

[8] C. G. Tang, "An Analysis of Baseline Distortion and Offset in NMR Spectra," *Journal of Magnetic Resonance, Series A,* vol. 109, no. 2, pp. 232-240, 1994/08/01/ 1994, doi: https://doi.org/10.1006/jmra.1994.1160.

[9] G. L. Chadzynski and U. Klose, "High Resolution Chemical Shift Imaging of the Human Brain without Water Suppression at 3T," in *World Congress on Medical Physics and Biomedical Engineering, September 7 - 12, 2009, Munich, Germany*, Berlin, Heidelberg, O. Dössel and W. C. Schlegel, Eds., 2009// 2009: Springer Berlin Heidelberg, pp. 177-180.

[10] S. Posse, R. Otazo, S. R. Dager, and J. Alger, "MR spectroscopic imaging: Principles and recent advances," *Journal of Magnetic Resonance Imaging,* vol. 37, no. 6, pp. 1301-1325, 2013, doi: https://doi.org/10.1002/jmri.23945.

[11] M. Wilson, "Adaptive baseline fitting for 1 H MR spectroscopy analysis," *Magn Reson Med,* vol. 85, no. 1, pp. 13-29, Jan 2021, doi: 10.1002/mrm.28385.

[12] Q. Bao *et al.*, "A new automatic baseline correction method based on iterative method," *J Magn Reson,* vol. 218, pp. 35-43, May 2012, doi: 10.1016/j.jmr.2012.03.010.

[13] W. Dou *et al.*, "Convex-Envelope Based Automated Quantitative Approach to Multi-Voxel 1H-MRS Applied to Brain Tumor Analysis," *PLOS ONE,* vol. 10, no. 9, p. e0137850, 2015, doi: 10.1371/journal.pone.0137850.

[14] Z. M. Zhang, S. Chen, and Y. Z. Liang, "Baseline correction using adaptive iteratively reweighted penalized least squares," *Analyst,* vol. 135, no. 5, pp. 1138-46, May 2010, doi: 10.1039/b922045c.

[15] M. Wilson, G. Reynolds, R. A. Kauppinen, T. N. Arvanitis, and A. C. Peet, "A constrained least-squares approach to the automated quantitation of in vivo (1)H magnetic resonance spectroscopy data," *Magn Reson Med,* vol. 65, no. 1, pp. 1-12, Jan 2011, doi: 10.1002/mrm.22579.

[16] Y. Zhang and J. Shen, "Smoothness of in vivo spectral baseline determined by mean-square error," *Magn Reson Med,* vol. 72, no. 4, pp. 913-22, Oct 2014, doi: 10.1002/mrm.25013.

[17] J. Near *et al.*, "Preprocessing, analysis and quantification in single-voxel magnetic resonance spectroscopy: experts' consensus recommendations," *NMR Biomed,* vol. 34, no. 5, p. e4257, May 2021, doi: 10.1002/nbm.4257.

[18] J. M. Tognarelli *et al.*, "Magnetic Resonance Spectroscopy: Principles and Techniques: Lessons for Clinicians," *J Clin Exp Hepatol,* vol. 5, no. 4, pp. 320-8, Dec 2015, doi: 10.1016/j.jceh.2015.10.006.

[19] L. G. Hanson, "Is quantum mechanics necessary for understanding magnetic resonance?," *Concepts in Magnetic Resonance Part A,* vol. 32A, no. 5, pp. 329-340, 2008, doi: https://doi.org/10.1002/cmr.a.20123.

[20] K. Belkić, "Magnetic Resonant Spectroscopy and Spectroscopic Imaging: A Review of Basic Principles and Recent Achievements in Oncology," *Journal of Computational*

Methods in Sciences and Engineering, vol. 3, pp. 505-533, 2003, doi: 10.3233/JCM-2003-3403.

[21] M. A. McLean, "3.16 - Fundamentals of MR Spectroscopy," in *Comprehensive Biomedical Physics*, A. Brahme Ed. Oxford: Elsevier, 2014, pp. 257-271.

[22] P. B. Barker, A. Bizzi, N. De Stefano, R. Gullapalli, and D. D. M. Lin, "Pulse sequences and protocol design," in *Clinical MR Spectroscopy*, 2009, ch. 2, pp. 19-33.

[23] R. Faghihi *et al.*, "Magnetic Resonance Spectroscopy and its Clinical Applications: A Review," *Journal of Medical Imaging and Radiation Sciences,* vol. 48, no. 3, pp. 233-253, 2017/09/01/ 2017, doi: https://doi.org/10.1016/j.jmir.2017.06.004.

[24] W. Bogner, R. Otazo, and A. Henning, "Accelerated MR spectroscopic imaging—a review of current and emerging techniques," *NMR in Biomedicine,* vol. 34, no. 5, p. e4314, 2021, doi: https://doi.org/10.1002/nbm.4314.

[25] E. L. Hahn, "Spin Echoes," *Physical Review,* vol. 80, no. 4, pp. 580-594, 11/15/ 1950, doi: 10.1103/PhysRev.80.580.

[26] R. Kreis *et al.*, "Terminology and concepts for the characterization of in vivo MR spectroscopy methods and MR spectra: Background and experts' consensus recommendations," *NMR in Biomedicine,* vol. 34, no. 5, p. e4347, 2021, doi: https://doi.org/10.1002/nbm.4347.

[27] J. B. Poullet, D. M. Sima, and S. Van Huffel, "MRS signal quantitation: a review of time- and frequency-domain methods," *J Magn Reson,* vol. 195, no. 2, pp. 134-44, Dec 2008, doi: 10.1016/j.jmr.2008.09.005.

[28] H. H. Lee and H. Kim, "Parameterization of spectral baseline directly from short echo time full spectra in 1H-MRS," *Magnetic Resonance in Medicine,* vol. 78, no. 3, pp. 836-847, 2017, doi: https://doi.org/10.1002/mrm.26502.

[29] C. Cudalbu *et al.*, "Contribution of macromolecules to brain 1H MR spectra: Experts' consensus recommendations," *NMR in Biomedicine,* vol. 34, no. 5, p. e4393, 2021, doi: https://doi.org/10.1002/nbm.4393.

[30] R. Birch, A. C. Peet, H. Dehghani, and M. Wilson, "Influence of macromolecule baseline on 1H MR spectroscopic imaging reproducibility," *Magnetic Resonance in Medicine,* vol. 77, no. 1, pp. 34-43, 2017, doi: https://doi.org/10.1002/mrm.26103.

[31] R. Kreis, "Issues of spectral quality in clinical 1H-magnetic resonance spectroscopy and a gallery of artifacts," *NMR Biomed,* vol. 17, no. 6, pp. 361-81, Oct 2004, doi: 10.1002/nbm.891.

[32] S. W. Provencher, "Estimation of metabolite concentrations from localized in vivo proton NMR spectra," *Magnetic Resonance in Medicine,* vol. 30, no. 6, pp. 672-679, 1993, doi: https://doi.org/10.1002/mrm.1910300604.

[33] K. Young, B. J. Soher, and A. A. Maudsley, "Automated spectral analysis II: Application of wavelet shrinkage for characterization of non-parameterized signals," *Magnetic Resonance in Medicine,* vol. 40, no. 6, pp. 816-821, 1998, doi: https://doi.org/10.1002/mrm.1910400606.

[34] H. Ratiney, Y. Coenradie, S. Cavassila, D. van Ormondt, and D. Graveron-Demilly, "Time-domain quantitation of 1H short echo-time signals: background accommodation," *Magnetic Resonance Materials in Physics, Biology and Medicine,* vol. 16, no. 6, pp. 284-296, 2004/05/01 2004, doi: 10.1007/s10334-004-0037-9.

[35] W. Dietrich, C. H. Rüdel, and M. Neumann, "Fast and precise automatic baseline correction of one- and two-dimensional nmr spectra," *Journal of Magnetic Resonance (1969),* vol. 91, no. 1, pp. 1-11, 1991/01/01/ 1991, doi: https://doi.org/10.1016/0022-2364(91)90402-F.

[36] D. E. Brown, "Fully Automated Baseline Correction of 1D and 2D NMR Spectra Using Bernstein Polynomials," *Journal of Magnetic Resonance, Series A,* vol. 114, no. 2, pp. 268-270, 1995/06/01/ 1995, doi: https://doi.org/10.1006/jmra.1995.1138.

[37] S. Golotvin and A. Williams, "Improved baseline recognition and modeling of FT NMR spectra," *J Magn Reson,* vol. 146, no. 1, pp. 122-5, Sep 2000, doi: 10.1006/jmre.2000.2121.

[38] D. Chang, C. D. Banack, and S. L. Shah, "Robust baseline correction algorithm for signal dense NMR spectra," *J Magn Reson,* vol. 187, no. 2, pp. 288-92, Aug 2007, doi: 10.1016/j.jmr.2007.05.008.

[39] S. W. Provencher, "Automatic quantitation of localized in vivo 1H spectra with LCModel," *NMR Biomed,* vol. 14, no. 4, pp. 260-4, Jun 2001, doi: 10.1002/nbm.698.

[40] J. B. Poullet *et al.*, "An automated quantitation of short echo time MRS spectra in an open source software environment: AQSES," *NMR Biomed,* vol. 20, no. 5, pp. 493-504, Aug 2007, doi: 10.1002/nbm.1112.

[41] P. Gillies, I. Marshall, M. Asplund, P. Winkler, and J. Higinbotham, "Quantification of MRS data in the frequency domain using a wavelet filter, an approximated Voigt lineshape model and prior knowledge," *NMR Biomed,* vol. 19, no. 5, pp. 617-26, Aug 2006, doi: 10.1002/nbm.1060.

[42] S. De Sanctis *et al.*, "Singular spectrum analysis for an automated solvent artifact removal and baseline correction of 1D NMR spectra," *J Magn Reson,* vol. 210, no. 2, pp. 177-83, Jun 2011, doi: 10.1016/j.jmr.2011.03.001.

[43] A. J. Wright and A. Heerschap, "Simple baseline correction for 1H MRSI data of the prostate," *Magn Reson Med,* vol. 68, no. 6, pp. 1724-30, Dec 2012, doi: 10.1002/mrm.24182.

[44] M. A. Parto Dezfouli, M. P. Dezfouli, and H. S. Rad, "A novel approach for baseline correction in 1H-MRS signals based on ensemble empirical mode decomposition," (in eng), *Annu Int Conf IEEE Eng Med Biol Soc,* vol. 2014, pp. 3196-9, 2014, doi: 10.1109/embc.2014.6944302.

[45] J. C. Cobas, M. A. Bernstein, M. Martin-Pastor, and P. G. Tahoces, "A new general-purpose fully automatic baseline-correction procedure for 1D and 2D NMR data," *J Magn Reson,* vol. 183, no. 1, pp. 145-51, Nov 2006, doi: 10.1016/j.jmr.2006.07.013.

[46] O. Bazgir, S. Mitra, B. Nutter, and E. Walden, "Fully Automatic Baseline Correction in Magnetic Resonance Spectroscopy," presented at the 2018 IEEE Southwest Symposium on Image Analysis and Interpretation (SSIAI), 2018.

[47] J. Slotboom, C. Boesch, and R. Kreis, "Versatile frequency domain fitting using time domain models and prior knowledge," *Magnetic Resonance in Medicine,* vol. 39, no. 6, pp. 899-911, 1998, doi: https://doi.org/10.1002/mrm.1910390607.